



# LUND UNIVERSITY

## Development of Novel Diffusion NMR Methods Preclinical Applications in Colloidal Model Systems Eriksson, Stefanie

2016

[Link to publication](#)

*Citation for published version (APA):*

Eriksson, S. (2016). *Development of Novel Diffusion NMR Methods: Preclinical Applications in Colloidal Model Systems*. Lund University, Faculty of Science, Center for Chemistry and Chemical Engineering.

*Total number of authors:*

1

### General rights

Unless other specific re-use rights are stated the following general rights apply:

Copyright and moral rights for the publications made accessible in the public portal are retained by the authors and/or other copyright owners and it is a condition of accessing publications that users recognise and abide by the legal requirements associated with these rights.

- Users may download and print one copy of any publication from the public portal for the purpose of private study or research.
- You may not further distribute the material or use it for any profit-making activity or commercial gain
- You may freely distribute the URL identifying the publication in the public portal

Read more about Creative commons licenses: <https://creativecommons.org/licenses/>

### Take down policy

If you believe that this document breaches copyright please contact us providing details, and we will remove access to the work immediately and investigate your claim.

LUND UNIVERSITY

PO Box 117  
221 00 Lund  
+46 46-222 00 00



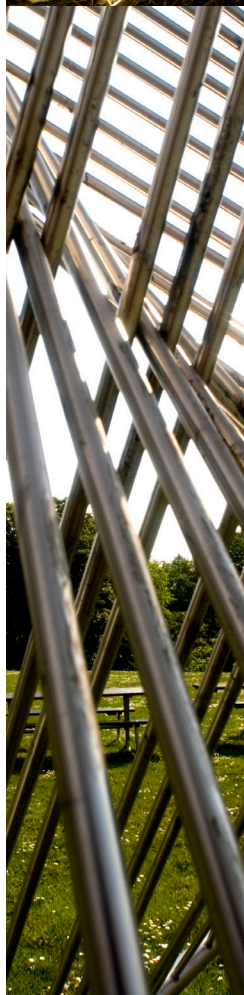
# Development of Novel Diffusion NMR Methods

Preclinical Applications in Colloidal Model Systems

---

STEFANIE ERIKSSON

PHYSICAL CHEMISTRY | FACULTY OF SCIENCE | LUND UNIVERSITY



# Development of Novel Diffusion NMR Methods

## Preclinical Applications in Colloidal Model Systems

Stefanie Eriksson



**LUND**  
UNIVERSITY

DOCTORAL DISSERTATION

Faculty opponent: Dr. Itamar Ronen, Leiden University Medical Center,  
Leiden, Netherlands

To be presented, with the permission of the Faculty of Science of Lund University, for public criticism on  
Friday the 27th of May 2016 at 13:15, in lecture hall A at the Center for Chemistry and Chemical  
Engineering, Lund.

Organization <b>LUND UNIVERSITY</b> Center for Chemistry and Chemical Engineering Lund		Document name <b>DOCTORAL DISSERTATION</b>	
		Date of disputation 2016-05-27	
Author(s) <b>Stefanie Eriksson</b>		Sponsoring organization Vetenskapsrådet	
Title and subtitle Development of Novel Diffusion NMR Methods: Preclinical Applications in Colloidal Model Systems			
Abstract <p>NMR is a powerful non-invasive technique utilizing radiofrequency and gradient pulses to manipulate the spins of atomic nuclei. In particular, diffusion NMR uses strong magnetic field gradients to label the positions of spins allowing for the measurement of translational motion of molecules in liquids. The average displacement of water molecules can give information on the pore microstructure in various materials including biological cells and tissues.</p> <p>The interpretation of conventional diffusion NMR signal can be ambiguous, as it contains effects from microstructure, size and orientation. In this work, the underlying microscopic structures are exposed with novel diffusion NMR methods. q-MAS is a pulse sequence for isotropic diffusion encoding, which in combination with conventional diffusion NMR can be used to quantify the microscopic anisotropy. The shape of the microscopic diffusion tensor can be revealed by varying the anisotropy of the diffusion encoding. The methods are demonstrated in lyotropic liquid crystals and yeast cell suspensions.</p> <p>Diffusion NMR can be used to measure exchange between intra- and extracellular compartments. This can give information on the water transport across biological cell membranes. A method for measuring exchange in yeast cells with different intra- and extracellular <math>T_2</math> values is presented.</p>			
Key words Diffusion NMR, diffusion tensor, microscopic anisotropy, q-MAS, exchange, liquid crystals, yeast cell suspensions			
Classification system and/or index terms (if any)			
Supplementary bibliographical information		Language English	
ISSN and key title		ISBN 978-91-7623-824-0 (print) 978-91-7623-825-7 (pdf)	
Recipient's notes		Number of pages 131	Price
		Security classification	

I, the undersigned, being the copyright owner of the abstract of the above-mentioned dissertation, hereby grant to all reference sources the permission to publish and disseminate the abstract of the above-mentioned dissertation.

Signature 

Date 2016-04-20



# Development of Novel Diffusion NMR Methods

Preclinical Applications in  
Colloidal Model Systems

Stefanie Eriksson



**LUND**  
UNIVERSITY

**Cover:** Detailed images from the Lund area: Tree with lights (Kennet Ruona), tubes in spiral (Gunnar Menander), cobblestone (Johan Persson).

© Stefanie Eriksson 2016

Faculty of Science, Center for Chemistry and Chemical Engineering

ISBN: 978-91-7623-824-0 (print)

ISBN: 978-91-7623-825-7 (pdf)

Printed in Sweden by Media-Tryck, Lund University, Lund 2016



*"Small shifts in your thinking, and small changes in your energy,  
can lead to massive alterations of your end result."  
-Kevin Michel*





## Acknowledgements

There are some people I'd like to thank, for helping me in one way or another, during the last 4.5 years.

First of all, I want to thank my supervisor Daniel Topgaard, for letting me be a part of this interesting research, for giving me the opportunity to travel and for encouraging me to try new things. I've learned a lot during these years.

Thank you Samo Lasič, my co-supervisor, for all your help, for always taking the time to discuss and for exchanging thoughts.

Olle Söderman, also my co-supervisor, thanks for your kind help and for the fruitful discussions on the basic stuff.

Thank you Patrik Galvosas and the other guys at Victoria, for letting me work in your lab and for making me feel so welcomed.

Thanks to all the people at the division of Physical Chemistry, for contributing to a great environment for research and fun. Thank you especially for the discussions on NMR: Jenny Algotsson, Sanna Gustavsson, Dat Pham, Tiago Ferreira, Diana Bernin, João Martins and Emelie Nilsson.

Thank you Ulf Olsson, Håkan Wennerström, Manja Berhrens and Kazuhiro Ishikawa, for the collaboration on the microemulsions, it was fun.

A huge thanks to the administrating staff at PhysChem for all the help through the years: thank you Majlis, Ingrid and Helena for making things

run smooth; thank you Maria for your great help with chemicals and supplies; thank you Christopher, for all your technical support.

Thank you Göran Carlström, for always being available to help with things concerning the magnets.

Thank you Simon Blazy, Johan Larsson and Mikael Novén, I really enjoyed helping you during your diploma work.

Thanks to my collaborators at BMC, Karin Lindkvist and Karin Elbing, thank you for the yeast.

Thanks to the people in the diffusion sphere: Karin Bryskhe and Carl-Fredrik Westin for organizing super interesting meetings; and to the people down the road: Markus Nilsson, Filip Szczepankiewicz, Björn Lampinen and André Ahlgren, thank you for all the fun times, diffusion MRI would not be the same without you.

Thanks to my dear friends: Tuva, for sharing lunches and PhD-student hacks; Lina, for sharing your wisdom on life.

Thanks to my family: Mamma och Pappa, for all the love and support; Joachim, thank you for being my brother.

Finally, thank you Stefan, for all your help with this book, thank you for loving me and for putting up with me during my ups and downs.

# Contents

<b>List of publications</b>	<b>xi</b>
<b>List of contributions</b>	<b>xiii</b>
<b>Populärvetenskaplig sammanfattning</b>	<b>xv</b>
<b>1 Introduction</b>	<b>1</b>
<b>2 Diffusion</b>	<b>3</b>
2.1 Brownian motion . . . . .	3
2.2 Diffusion propagator . . . . .	5
2.3 Diffusion tensor . . . . .	6
2.3.1 Microscopic vs. macroscopic anisotropy . . . . .	8
2.4 Exchange . . . . .	9
<b>3 Nuclear Magnetic Resonance</b>	<b>11</b>
3.1 The NMR signal . . . . .	11
3.2 The RF-pulse . . . . .	13
3.3 The NMR spectrum . . . . .	14
3.4 Relaxation . . . . .	15
3.4.1 Inversion recovery . . . . .	15
3.4.2 Spin Echo . . . . .	16
3.5 Magnetic field gradients . . . . .	17
3.6 Diffusion NMR . . . . .	18
3.6.1 Conventional diffusion encoding . . . . .	18

## Contents

---

3.7	Imaging . . . . .	22
3.7.1	Diffusion tensor imaging . . . . .	22
<b>4</b>	<b>Colloidal model systems</b>	<b>25</b>
4.1	Surfactants . . . . .	25
4.1.1	Lyotropic liquid crystals . . . . .	27
4.2	Characterizations of liquid crystals . . . . .	28
4.2.1	SAXS . . . . .	28
4.2.2	$^2\text{H}$ NMR . . . . .	28
4.3	Yeast cells . . . . .	29
4.3.1	Aquaporins . . . . .	30
<b>5</b>	<b>Diffusion NMR for microscopic anisotropy</b>	<b>31</b>
5.1	Conventional diffusion encoding . . . . .	31
5.2	More encoding directions . . . . .	33
5.3	Isotropic diffusion encoding . . . . .	33
5.4	$q$ -MAS - magic angle spinning of the $q$ -vector . . . . .	34
5.5	Quantifying microscopic anisotropy with isotropic diffusion weighting . . . . .	35
5.6	Prolate or oblate? . . . . .	38
<b>6</b>	<b>Diffusion NMR for exchange</b>	<b>41</b>
6.1	Conventional diffusion encoding in a two-compartment system . . . . .	41
6.2	Methods to study exchange with diffusion NMR . . . . .	42
6.2.1	Kärger model . . . . .	42
6.2.2	Filter exchange spectroscopy . . . . .	45
6.3	Accounting for differences in relaxation rates in FEXSY . . . . .	46
6.3.1	Operator analysis for signal evolution . . . . .	47
<b>7</b>	<b>Concluding remarks</b>	<b>51</b>
	<b>References</b>	<b>53</b>



# List of publications

This thesis is based on the following publications, referred to by their Roman numerals:

- I **Stefanie Eriksson**, Samo Lasič and Daniel Topgaard. **Isotropic diffusion weighting in PGSE NMR by magic-angle spinning of the q-vector.** *Journal of Magnetic Resonance*, 226:13–18, 2013
- II Samo Lasič, Filip Szczepankiewicz, **Stefanie Eriksson**, Markus Nilsson and Daniel Topgaard. **Microanisotropy imaging: quantification of microscopic diffusion anisotropy and orientational order parameter by diffusion MRI with magic-angle spinning of the q-vector.** *Biophysics*, 2:11, 2014
- III **Stefanie Eriksson**, Samo Lasič, Markus Nilsson, Carl-Fredrik Westin and Daniel Topgaard. **NMR diffusion-encoding with axial symmetry and variable anisotropy: Distinguishing between prolate and oblate microscopic diffusion tensors with unknown orientation distribution.** *The Journal of Chemical Physics*, 142(10):104201, 2015
- IV **Stefanie Eriksson**, Karin Elbing, Olle Söderman, Karin Lindkvist, Daniel Topgaard and Samo Lasič. **NMR Quantification of Exchange Between Compartments with Different Relaxation Rates.** *Manuscript*

All papers are reproduced with permission of their respective publishers.

## Publication not included in this thesis:

- Ishikawa, Kazuhiro, Manja Behrens, **Stefanie Eriksson**, Daniel Topgaard, Ulf Olsson, and Håkan Wennerström. **Microemulsions of Record Low Amphiphile Concentrations Are Affected by the Ambient Gravitational Field.** *The Journal of Physical Chemistry B*, 2016



# List of contributions

- **Paper I** I took part in performing the experiments and carried out the analysis. I was responsible for writing parts of the paper.
- **Paper II** I took part in performing the NMR experiments and carried out the analysis. I was responsible for writing parts of the paper.
- **Paper III** I made the samples. I analyzed the SAXS data. I took part in performing the NMR experiments. I was responsible for writing parts of the paper.
- **Paper IV** I set up and ran the experiments, I developed the method together with Samo Lasič, and I did the analysis. I was responsible for writing the manuscript.





# Populärvetenskaplig sammanfattning

Kärnmagnetisk resonans, NMR, är en teknik som har många användningsområden, inte minst används NMR som en bildgivande teknik för diagnostisering av skador och sjukdomar, vilket görs med så kallade MR-kameror. Med hjälp av diffusions-NMR kan man mäta vattenmolekylers rörelse, d.v.s. vattnets *diffusion*. Diffusions-NMR gör det möjligt att mäta hur långt vattenmolekylerna rör sig i olika riktningar. Diffusion kallas för *anisotropisk* om molekyler har möjlighet att förflytta sig långa sträckor i en riktning, men bara kortare sträckor i en annan riktning. Anisotropisk diffusion kan användas för avbildning av *mikroskopiska strukturer*, till exempel nervfibrer i vit hjärnvävnad. Nervfibrerna kan liknas vid långa rör där vattnet inuti röret kan förflytta sig fritt i riktningen längs med röret, men stoppas från att förflytta sig i vinkelrät riktning. Nervfibrerna i hjärnan är mycket mindre än upplösningen i MR-kameran och det kan finnas många fibrer i ett och samma bildgivande volymelement, *voxel*. Om de olika nervfibrerna inuti en voxel har flera olika riktningar, kan det verka som att vattnet diffunderar lika mycket i alla riktningar och det mikroskopiska strukturerna kan inte bli detekterade med vanlig diffusions-NMR.

I detta arbete har nya metoder för att påvisa förekomsten av mikroskopisk anisotropi utvecklats, även i de situationer då strukturerna har flera olika riktningar. Dessa metoder har utvärderats i så kallade *flytande kristaller* som kan tillverkas genom att blanda surfaktanter och vatten.

Ett annat bra modelsystem, för utvärdering av diffusions-NMR, är jäst utblandat i vatten. Jästcellerna liknar mänskliga celler på många sätt. Vattenmolekylerna utanför cellerna kan röra sig fritt, medan vattenmolekylerna inuti stoppas av cellmembranet. Diffusions-NMR kan detektera både vattnet som rör sig fritt och vattnet som är instängt i cellen. I detta arbete har diffusions-NMR används för att mäta hur vatten transporteras genom cellmembranet i speciella genmodifierade jästceller.



# 1

## Introduction

Water is the most abundant molecule in the human body and it is present in most human cells and tissues. Water molecules are moving randomly through Brownian motion. Displacement of the water molecules is affected by cell structure. Hence, measuring this motion can give structural information on the system.

Diffusion NMR (nuclear magnetic resonance) is a powerful tool that can measure the translational motion of molecules in liquids.<sup>1</sup> This technique allows the microscopic structure of porous materials to be studied and can give information on the shape and size of the pores in *e.g.* liquid crystals,<sup>2</sup> rocks<sup>3</sup> and cellulose fibers<sup>4</sup>. Diffusion MRI (magnetic resonance imaging) can be applied in the brain, where the white brain matter fibres are structures that render the water diffusion anisotropic.<sup>5</sup> The white brain matter consists of axons surrounded by myelin sheets,<sup>6</sup> which act as protection of the axon. The myelinated axons can be thought of as tubes where the internal water can diffuse freely along the direction of the tube but is restricted in the perpendicular direction. Many myelinated axons bundle together and form connections between different parts of the brain.<sup>7</sup> These anisotropic structures can be imaged with diffusion tensor imaging, DTI, where the diffusion anisotropy inside the voxels is quantified. Changes of the quantified anisotropy in the brain has been connected to different disorders *e.g.* autism, schizophrenia, Alzheimer's and multiple sclerosis.<sup>6;8</sup> One problem with DTI is that it is affected by the orientation distribution of the microscopic structures inside the imaging voxels, for example when there are crossing fibres. In this thesis, Paper I, II and III present novel diffusion NMR methods for disentangling pore structure from orientation distributions, on a subvoxel scale. Proof-of-principle experiments are performed on lyotropic liquid

## 1 Introduction

---

crystals and yeast cells.

In cells with permeable walls the water can exchange between the intra- and extracellular compartments. The transport of water across the cell membrane is usually facilitated by special water transport proteins, so called aquaporins.<sup>9;10</sup> Diffusion NMR can be used to study this type of molecular exchange.<sup>11</sup> The water in the intra- and extracellular compartments can have different diffusivities as well as different relaxation times, which will affect the NMR signal. In Paper IV a diffusion NMR method is presented that allows the measurement of molecular exchange in the presence of different  $T_2$  values in the intra- and extracellular compartments. The method is demonstrated on yeast cells with and without aquaporins in the cell membrane.

# 2

## Diffusion

### 2.1 Brownian motion

Diffusion is the translational motion of particles, which occurs in all liquids and gases and is driven by thermal energy. The induced random motion of the particles is called Brownian motion, and is caused by constant inter-particle collisions. One single particle may have one direction and velocity at one moment and yet a completely other direction and velocity in the next.

As it is impossible to predict the exact path for every single particle, due to the large amount of particles in the system, it can be convenient to model the trajectory statistically with the so called random walk. In the random walk model each step has a length,  $\lambda$ , and the time for each step is  $\tau$ . Furthermore, the direction of each step is completely random and there is no correlation in direction between consecutive steps.



**Figure 2.1:** The three dimensional trajectory of one particle with starting position  $\mathbf{r}_0$  at the center of the sphere and end position  $\mathbf{r}_1$ . The displacement during time  $t$  is  $\mathbf{R} = \mathbf{r}_1 - \mathbf{r}_0$ .

By using this model, the trajectory for a particle starting at a position  $\mathbf{r}_0$  and diffusing for a time  $t$  can be simulated. The end position is  $\mathbf{r}_1$  and its translation is  $\mathbf{R} = \mathbf{r}_1 - \mathbf{r}_0$ . In Fig. 2.1 an example of a three dimensional trajectory of a single particle is shown.

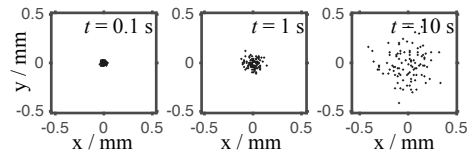
## 2 Diffusion

For three dimensions the diffusion coefficient  $D$  is related to the step length and the time for each step according to<sup>12</sup>

$$D = \frac{\lambda^2}{6\tau}. \quad (2.1)$$

The trajectories in an ensemble of particles starting at the same position, is different for each particle and thus, the particles spread out over time. In Fig. 2.2 the positions of 100 particles in the  $xy$ -plane at three different time points are shown. All particles start at the same position and spread out more the longer they diffuse.

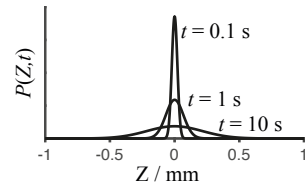
**Figure 2.2:** An ensemble of 100 particles, with diffusion coefficient,  $D = 2.3 \cdot 10^{-9} \text{ m}^2\text{s}^{-1}$  all starting at the same position at  $t = 0$ . The particles spread out more with increasing time,  $t$ .



In one dimension the probability density for a particle to move a distance  $Z$  during the time  $t$  is given by<sup>12</sup>

$$P(Z, t) = \left( \frac{2\tau}{\pi t \lambda^2} \right)^{1/2} \exp \left( -\frac{Z^2 \tau}{2t \lambda^2} \right). \quad (2.2)$$

**Figure 2.3:** One-dimensional probability densities.  $P(Z, t)$  show the probability for finding a particle at a distance  $Z = z_1 - z_0$  from its starting position at time  $t$ .



For spherical particles in a liquid,  $D$  depends on the thermal energy  $k_B T$ , the viscosity  $\eta$  of the liquid, and the hydrodynamic radius of the particle  $R_H$ , according to the Stokes-Einstein equation

$$D = \frac{k_B T}{6\pi\eta R_H}, \quad (2.3)$$

where  $k_B$  is the Boltzmann constant,  $T$  is the temperature.<sup>13</sup>

## 2.2 Diffusion propagator

In a macroscopic system, diffusion can be thought of as the flux of particles from an area with high concentration to an area with low concentration. Fick's first law relates the diffusion coefficient to the flux of particles,  $\mathbf{J}$ , in a system with a concentration gradient  $\nabla c$ ,

$$\mathbf{J}(\mathbf{r}, t) = -D\nabla c(\mathbf{r}, t). \quad (2.4)$$

Fick's second law connects the change in concentration with time, to the diffusion coefficient  $D$  and the second derivative of the local concentration,

$$\frac{\partial c(\mathbf{r}, t)}{\partial t} = D\nabla^2 c(\mathbf{r}, t). \quad (2.5)$$

In the case of self-diffusion there is no concentration gradient and diffusion is described by the propagator  $P(\mathbf{R}, t)$ , which is the probability for a particle to move a distance  $\mathbf{R} = \mathbf{r}_1 - \mathbf{r}_0$  during time,  $t$ . For free diffusion in a homogeneous medium the propagator is given by a Gaussian function,<sup>14</sup>

$$P(\mathbf{R}, t) = (4\pi Dt)^{-3/2} \exp\left(-\frac{(\mathbf{r}_1 - \mathbf{r}_0)^2}{4Dt}\right). \quad (2.6)$$

In the case of Gaussian diffusion, the self-diffusion coefficient of a specific component can be determined by the mean square displacement in one direction, according to

$$\langle Z^2 \rangle = 2Dt \quad (2.7)$$

In a heterogeneous system the propagator will depend on the local particle density,  $\rho(\mathbf{r}_0)$ . The average propagator is achieved by integration over all starting positions  $\mathbf{r}_0$ <sup>14</sup>

$$P(\mathbf{R}, t) = \int \rho(\mathbf{r}_0) P(\mathbf{r}_0, \mathbf{r}_0 + \mathbf{R}, t) d\mathbf{r}_0, \quad (2.8)$$

The mean square displacement, MSD, shown in Eq. 2.7 is only valid for free diffusion. In cases of obstructed and restricted diffusion  $\text{MSD} \leq 2Dt_D$ , where  $t_D$  is the diffusion time. In Fig. 2.4 free and restricted diffusion are compared at different  $t_D$ . At short  $t_D$

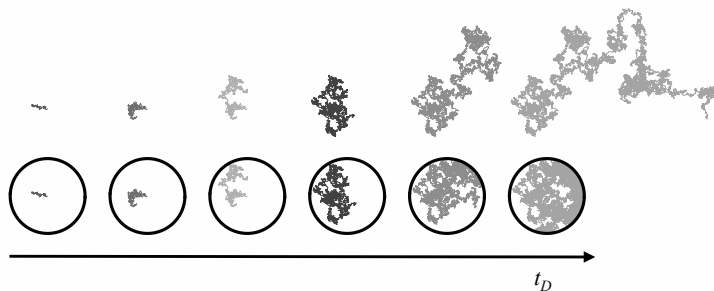


**Figure 2.4:** Simulated free (upper panel) and restricted (lower panel) diffusion. All trajectories are from the same simulated particle but at different diffusion times  $t_D$ , indicated by the different gray scales. The upper and lower trajectories become different when the particle hit the circular wall. In the simulation the particle direction is reflected backward when it hits the wall.

the trajectories are the same for free and restricted diffusion but at longer  $t_D$  the restricted particles are stopped from moving further out, by the circular wall. Obstructed diffusion is when the path of the particle is hindered in some directions but it can move around the obstruction in some other direction.<sup>14</sup> If the free particles in Fig. 2.4 would move downward they would become obstructed by the circular wall. At long  $t_D$ , MSD of restricted molecules will be lower than of obstructed molecules, which in turn will be lower than MSD of freely diffusing molecules.<sup>15</sup>

Since Eq. 2.7 only holds for free diffusion it can be convenient to define an apparent diffusion coefficient, ADC, which is usually what is measured with NMR<sup>16</sup>

$$\text{ADC} = \frac{\langle Z^2 \rangle}{2t_D}. \quad (2.9)$$

### 2.3 Diffusion tensor

The mean square displacement can be dependent on direction rendering ADC anisotropic. Anisotropic diffusion can be described by a diffusion tensor<sup>17;18</sup>



$$\mathbf{D} = \begin{pmatrix} D_{xx} & D_{xy} & D_{xz} \\ D_{yx} & D_{yy} & D_{yz} \\ D_{zx} & D_{zy} & D_{zz} \end{pmatrix}. \quad (2.10)$$

which shows the apparent diffusivities for different directions in the laboratory coordinate system. The mean diffusivity is given by the trace of the diffusion tensor

$$\bar{D} = \text{Tr}(\mathbf{D})/3 = (D_{xx} + D_{yy} + D_{zz})/3 \quad (2.11)$$

By diagonalizing the diffusion tensor given in 2.10 diffusion can be described in the principal axis system of the studied sample and represented by an ellipsoid, as shown in Fig. 2.5, where the eigenvectors point along the principle axes of the studied sample. The eigenvalues  $\lambda_1$ ,  $\lambda_2$  and  $\lambda_3$  are the scalar values of the eigenvectors of the diffusion tensor in the principle axis coordinate system.

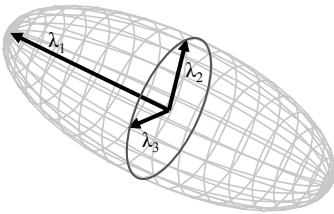


**Figure 2.5:** Anisotropic diffusion can be described by a diffusion tensor,  $\mathbf{D}$ , which has the form of an ellipsoid. The eigenvalues of  $\mathbf{D}$ ,  $\lambda_1$ ,  $\lambda_2$  and  $\lambda_3$ , are the scalar values of the tensor eigenvectors.

For an axially symmetric diffusion tensor there are always two eigenvalues that are equal. If the axis of symmetry is longer than the two other than the shape is called a prolate, if it is shorter it is called a oblate. Different diffusion tensor shapes are shown in a Fig. 2.6.

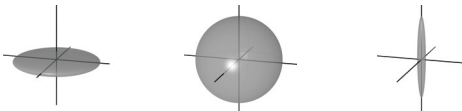


**Figure 2.6:** Three types of diffusion tensors shapes, from left to right: oblate, spherical and prolate. For oblate diffusion tensors, the relation between the eigenvalues are  $\lambda_1 = \lambda_2 > \lambda_3$ , for spherical shapes  $\lambda_1 = \lambda_2 = \lambda_3$  and for prolate shapes  $\lambda_1 > \lambda_2 = \lambda_3$ .

### 2.3.1 Microscopic vs. macroscopic anisotropy

If the MSD of an ensemble of particles, all starting at the same position, is different in different directions, then diffusion is anisotropic on a microscopic scale.<sup>19</sup> This is sometimes referred to as local anisotropy.<sup>20</sup> Microscopic anisotropy can be illustrated by considering diffusing molecules inside a cylinder. If the particles move in the direction of the cylinder axis, nothing will restrict their displacement, and MSD will be the same as in a bulk solution. On the other hand if the particles move in the direction perpendicular to the cylinder axis, the cylinder wall will stop further displacement and the MSD of the particles will be restricted by the cylinder wall.

Now consider a volume containing many cylinders. If the cylinders all have the same direction, the average MSD will be the same as in one cylinder and the diffusion is macroscopically anisotropic. However, if the cylinders are randomly oriented, the average MSD is the same in all directions and diffusion on a macroscopic scale is isotropic. If the volume instead contains spheres, the diffusion is the same in all directions and the microscopic diffusion is isotropic.

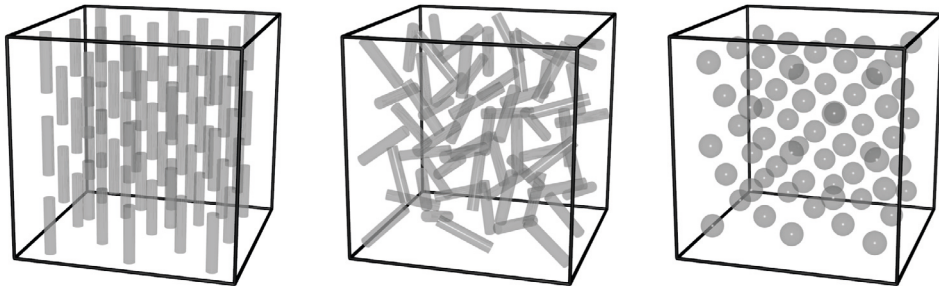


**Figure 2.7:** Three volumes containing different types of microscopic structures, cylinders and spheres. Diffusion is anisotropic inside the cylinders and isotropic inside the spheres. For a volume with cylinders, all oriented in the same direction, the diffusion is microscopically and macroscopically anisotropic. If the cylinders are randomly oriented, diffusion is microscopically anisotropic but macroscopically isotropic. For a volume containing spheres diffusion is microscopically and macroscopically isotropic.

## 2.4 Exchange

In heterogeneous systems, different regions can have different apparent diffusivities. There are several reasons for why diffusivities can differ between different compartments. For example, as was shown above the ADC can differ between regions with free, obstructed and restricted diffusion. Also in compartments with different orientations, the ADC can vary. Another reason is molecules that bind at specific sites while others diffuse freely.<sup>21</sup> If molecules move from one compartment to another, it is called molecular exchange. Fig. 2.8 shows illustrations of exchange between regions with different diffusivities. The exchange rate is given by

$$k = \frac{1}{\tau_1} + \frac{1}{\tau_2}, \quad (2.12)$$

where  $\tau_{1,2}$  is the average residence time of the molecule in respective compartment.

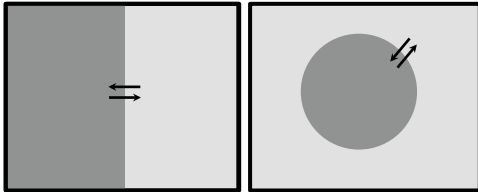


**Figure 2.8:** Two illustrations of exchange between environments with different diffusivities. The darker area represents low diffusivity and the higher area represents high diffusivity.



# 3

## Nuclear Magnetic Resonance

Nuclear magnetic resonance, NMR, was first demonstrated in 1938 by Rabi et al.<sup>22</sup> In the 1940's the technique was further developed by Felix Bloch<sup>23</sup> and Edward Purcell,<sup>24</sup> who were awarded the Nobel price in physics, 1952. Since then NMR has become a very diverse technique with many areas of application. In chemistry it is mostly used as a spectroscopic technique for studying the structure of molecules.<sup>25</sup> In healthcare, magnetic resonance imaging, MRI, is an important non-invasive imaging technique, mainly used for diagnostics.<sup>26</sup> NMR is also a powerful tool to measure translational motion of molecules.<sup>1</sup>

NMR utilizes the interaction between the magnetic moment of the atomic nuclei and external magnetic fields.<sup>27</sup>

### 3.1 The NMR signal

Spin is an intrinsic property, possessed by all atomic nuclei. The spin quantum number  $I$  of the nuclei, depends on the quarks that builds up the protons and neutrons in the nucleus.<sup>27</sup> Nuclei that possess a spin quantum number higher than zero,  $I > 0$ , have an intrinsic nuclear magnetic moment  $\mu$  which is required for a nuclear isotope to be NMR compatible. Another important aspect of NMR compatibility is the abundance of the specific isotope in nature. The most abundant isotope is the proton,  $^1\text{H}$ , which can be found almost everywhere in nature, especially in normal water,  $\text{H}_2\text{O}$ . Protons have spin quantum number  $I = 1/2$ . For some isotopes that are not naturally abundant in nature, such as deuterium,  $^2\text{H}$ , isotopic enrichment is necessary for it to be compatible with

### 3 Nuclear Magnetic Resonance

---

NMR.<sup>27</sup> Deuterium,  $^2\text{H}$ , has spin quantum number  $I = 1$ .

A nucleus with spin quantum number  $I$  can adopt  $2I + 1$  different states. For  $^1\text{H}$  there are two states and for  $^2\text{H}$  there are three states. In the absence of a magnetic field the energy levels of the different states are degenerate, *i.e.* equivalent. When a magnetic field is applied the energies of the states split into different levels, the so called Zeeman splitting, and the difference in energy depends on the type of nucleus and the magnetic field strength,  $B$

$$E = -m\hbar\gamma B, \quad (3.1)$$

where  $m$  is the magnetic quantum number,  $\hbar$  is Plank's constant divided with  $2\pi$  and  $\gamma$  is the gyromagnetic ratio. The transition from a higher energy state to a lower will generate energy,  $\Delta E = \hbar\gamma B$ , in the form of radiation.

The splitting of energy states can be thought of as the spins aligning in the external magnetic field. The spins can either align with the external field, (low energy state), or align opposite to the magnetic field (high energy state). However, since the spin is a quantum mechanical property the orientation of the magnetic moment is always a superposition of the different energy states. The spins are precessing around the applied magnetic field  $B_0$  with the Larmor frequency

$$\omega_0 = -\gamma B_0. \quad (3.2)$$

The aligned magnetic moments from an ensemble of spins, build up a macroscopic magnetization  $M_0$  in the direction of the main magnetic field,  $B_0$ , which can be seen in Fig 3.1. The strength of the magnetization is given by<sup>26</sup>

$$M_0 = \frac{\rho\gamma^2\hbar^2 B_0}{4k_B T} \quad (3.3)$$

where  $\rho$  is the spin density.

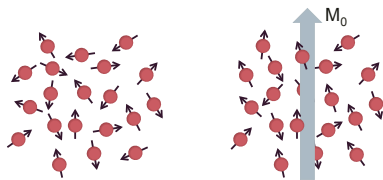


**Figure 3.1:** The magnetic moments of the nuclei are in random orientation when no magnetic field is applied. When the magnetic field is applied the magnetic moment of the spins align slightly along the direction of the field and a magnetization  $M_0$  is built up.

## 3.2 The RF-pulse

As long as the magnetization is aligned with the static magnetic field,  $B_0$ , which by convention is applied along the  $z$ -direction, it can not be measured. By applying an oscillating electro-magnetic field,  $B_1$ , a so called radio-frequency (RF) pulse, the magnetization vector,  $\mathbf{M}$ , can be manipulated and its orientation changes through nutation according to the Bloch equation:

$$\frac{d\mathbf{M}}{dt} = \mathbf{M} \times \gamma \mathbf{B}_1. \quad (3.4)$$

This equation is a semi classical representation of NMR and is most useful in our case. The  $B_1$  field is usually perpendicular to  $B_0$  and it causes  $\mathbf{M}$  to nutate down towards the  $xy$ -plane. The resulting orientation of the magnetisation vector after the RF-pulse, depends on the strength and duration of the latter. If the magnetization vector is rotated into the  $xy$ -plane, the RF-pulse is called a  $90^\circ$ -pulse. If it inverts the magnetization completely to the  $-z$ -direction it is called a  $180^\circ$ -pulse.

The RF-pulse is produced by a transmission coil that surrounds the sample, which can be seen in Fig. 3.2.

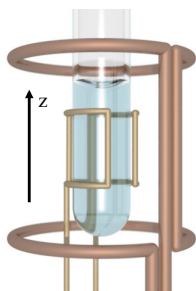


**Figure 3.2:** Illustration of a typical spectroscopic NMR set-up. The sample volume, surrounded by the inner coil, is irradiated by an RF-pulse, which excites the spins. The active volume is defined by the size of the RF-coil, which in normal NMR spectrometers is usually between 5-10 mm wide and about 5-10 mm long, but depending on the application, the RF-coil can also be much bigger. The outer coil generates a magnetic field gradient used for diffusion encoding and imaging, as discussed later. By convention the direction of the main magnetic field is always aligned with the  $z$ -direction.

### 3 Nuclear Magnetic Resonance

---

After the application of the  $90^\circ$ -pulse, the magnetization starts precessing and induces a current in the receiver coil surrounding the sample. The induced current can be detected as an oscillating signal, which is called the free induction decay (FID). The FID is decaying during acquisition because of relaxation.

When studying the behaviour of the magnetization vector as in Eq. 3.4, it is convenient to use the rotating frame instead of the laboratory frame.<sup>26</sup> The rotating frame rotates around the  $z$ -axis with the Larmor frequency  $\omega_0$ . In the rotating frame, a spin precessing with  $\omega_0$  is stationary and has a constant phase angle,  $\phi$ . In the continuation of this text, the rotating frame of reference will be used.

### 3.3 The NMR spectrum

A Fourier transform of the FID, gives a spectrum with peaks corresponding to the resonance frequencies of the spins in the sample.

Chemical shift,  $\delta_{cs}$ , is a small change in the resonance frequency of the spin, resulting from diamagnetic shielding of  $B_0$ , caused by the electrons in the atom surrounding the nuclei. The shielding is denoted  $\sigma$  and the new resonance frequency is given by

$$\omega = \gamma B_0(1 - \sigma) \quad (3.5)$$

The chemical shift is usually calculated as a shift from the resonance frequency of a reference compound,  $\omega_{ref}$ ,

$$\delta_{cs} = 10^6 \frac{\omega - \omega_{ref}}{\omega_{ref}}, \quad (3.6)$$

and is given in ppm (parts per million).

The chemical shift is independent of magnetic field strength and thus very convenient, as it is possible to compare spectra retrieved with different magnetic field strengths, where the same compound will always show the same  $\delta_{cs}$ .



## 3.4 Relaxation

Directly after the  $90^\circ$ -pulse the strength of the magnetization located in the  $xy$ -plane is given by Eq. 3.3. However, the magnetization  $xy$ -plane will start to decrease, causing the FID to decay. This happens through two different processes.

The first type of signal decay is the  $T_1$ - or longitudinal relaxation where the spin ensemble returns to thermal equilibrium. This process is also called spin-lattice relaxation, since the excited spins in this process transfer its energy to the surroundings, for example a lattice in the case of a solid.

The second type of signal decay is the  $T_2$ -relaxation, also called transverse relaxation or spin-spin relaxation.  $T_2$ -relaxation is, among other things, caused by dipolar interactions between spins. The spins can feel a fluctuating magnetic field caused by surrounding spins. This can induce a phase shift because of changing precession frequency. If the motion of the spins is fast and isotropic this effect will be averaged out to zero. This is why fluids often have longer  $T_2$ -relaxation than solids.<sup>1</sup>

There is also a second type of transverse relaxation commonly called  $T_2^*$ , which is caused by inhomogeneities in the magnetic field. This effect can be effectively reversed by the use of the Hahn-echo also called spin-echo,<sup>28</sup> which will be discussed later (see Fig 3.5).

The Bloch equations can be modified to include the effect of relaxation:

$$\begin{aligned} M_x(t) &= M_0 \sin(\omega_0 t) \exp(-t/T_2) \\ M_y(t) &= M_0 \cos(\omega_0 t) \exp(-t/T_2) \\ M_z(t) &= M_0 [1 - \exp(-t/T_1)]. \end{aligned} \quad (3.7)$$

In Fig. 3.3 the effects of  $T_1$  and  $T_2$  on the magnetization is shown. Two methods to determine  $T_1$  and  $T_2$  relaxation are shown in the sections below.

### 3.4.1 Inversion recovery

Inversion recovery is the standard method to measure  $T_1$  relaxation. The pulse sequence is shown in Fig. 3.4.<sup>1</sup> Here the magnetization is first inverted from the equilibrium  $+z$  direction to the  $-z$  axis by a  $180^\circ$ . During signal evolution the magnetization will

### 3 Nuclear Magnetic Resonance

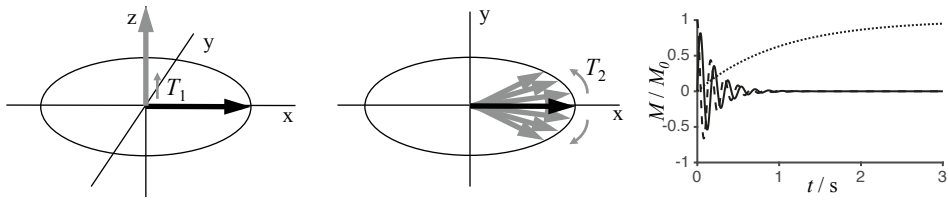


**Figure 3.3:** Change in magnetization due to relaxation. The left panel shows longitudinal relaxation,  $T_1$ , the middle panel shows transverse relaxation,  $T_2$ . The black arrow represents the magnetization vector directly after the  $90^\circ$ -pulse, grey arrows show the effect of relaxation. The right panel shows the magnetizations:  $M_x$  (solid line),  $M_y$  (dashed line) and  $M_z$  (dotted line) according to Eq. 3.7.

relax back towards equilibrium. After a time delay,  $\tau$ , the magnetization is flipped to the  $xy$ -plane with a  $90^\circ$ -pulse, after which the signal is detected. The amplitude of the magnetization in the  $xy$ -plane is given by

$$M(\tau) = M_0[1 - 2\exp(-\tau/T_1)] \quad (3.8)$$

By repeating the experiment for different values  $\tau$ ,  $T_1$  can be retrieved by fitting Eq. 3.8 to the data.

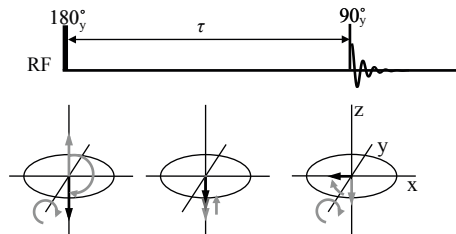


**Figure 3.4:** The inversion recovery pulse sequence and its effect on the magnetization vector. The grey arrows represents the magnetization before the RF-pulse and the black arrows represent the resulting magnetization vector. The  $180^\circ$ -pulse turns the magnetization around the  $y$ -axis and inverts it. During evolution time,  $\tau$ , the magnetization will relax through  $T_1$  relaxation, towards equilibrium. The  $90^\circ$ -pulse flips the magnetization back to the  $xy$ -plane where it can be detected.

#### 3.4.2 Spin Echo

$T_2$ -relaxation can be measured with the spin echo, shown in Fig. 3.5.<sup>28</sup> The spin echo itself is a very convenient method in diffusion and imaging sequences, because of its

ability to refocus magnetisation lost due to  $T_2^*$  relaxation. The  $90^\circ$ -pulse brings the magnetisation to the  $xy$ -plane where the magnetization vector evolves. After a time delay  $\tau$ , the magnetization inverted with the  $180^\circ$ -pulse. During the second delay, the signal will again evolve. After  $2\tau$  the dephasing caused by  $T_2^*$  is refocused and an echo is formed. The transverse relaxation caused by normal  $T_2$  relaxation is not refocused and the magnetisation decreases according to

$$M(2\tau) = M_0 \exp(-2\tau/T_2) \quad (3.9)$$

The experiment is repeated with different  $\tau$  and  $T_2$  is retrieved by fitting Eq. 3.9 to the data.

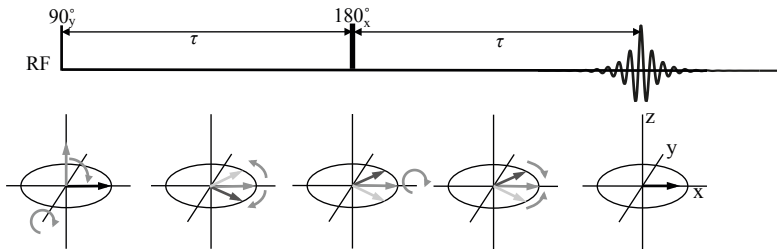


**Figure 3.5:** The spin echo pulse sequence and its effect on the magnetization vector. Before the first RF-pulse the magnetization is at equilibrium directed in the  $z$ -direction. The  $90^\circ$ -pulse turns the magnetization around the  $y$ -axis to the  $xy$ -plane where it ends up in the  $x$ -direction. During the first evolution time  $\tau$  the magnetization is affected by transverse relaxation. The  $180^\circ$ -pulse inverts the magnetization by turning it around the  $x$ -axis. During the second evolution time, dephasing caused by  $T_2^*$  will rephase and generate an echo after  $2\tau$ .

### 3.5 Magnetic field gradients

The application of magnetic field gradients induces a change in the magnetic field strength as a function of the position. For our purpose the gradient is kept constant in the sample and is generated by the gradient coils surrounding the sample (see Fig. 3.2).

If the magnetic field gradient is applied along the  $z$ -axis then the resulting magnetic field,  $B'_0(z)$ , will vary along the  $z$ -axis as

$$B'_0(z) = B_0 + gz. \quad (3.10)$$

Thus the precession frequency of the spins will depend on their position according to

$$\omega(z) = \gamma B_0 + \gamma gz. \quad (3.11)$$

In this way the positions of the spins can be labelled. This labelling is the basis for NMR diffusion and imaging.

## 3.6 Diffusion NMR

Diffusion NMR is a powerful tool, which uses magnetic field gradients to label the position and follow the translational motion of spins.<sup>1;29</sup> The method is very useful to measure self-diffusion coefficients of molecules and aggregates in liquids<sup>30</sup>. Another very useful application is probing the water diffusion in porous materials to retrieve information about the microscopic structure as well as pore size and shape. This can be done in many different types of materials, such as rocks, cellulose and liquid crystals.<sup>2-4</sup> It can also be used to elucidate white brain matter fibre tracts in the brain.<sup>31</sup>

### 3.6.1 Conventional diffusion encoding

Stejskal and Tanner first presented the diffusion method utilizing pulsed magnetic field gradients (PFG) in 1965.<sup>32</sup> The two most common experiments are the pulsed-gradient spin echo (PGSE)<sup>32</sup> and the pulsed-gradient stimulated echo (PGSTE),<sup>33</sup> shown in Fig. 3.6. The two sequences differ in the RF-pulses that generate the echo.

The PGSE sequence has one  $90^\circ$ -pulse that excites the spins and one  $180^\circ$ -pulse that inverts the magnetization and creates the echo. The PGSTE sequence utilizes three  $90^\circ$ -pulses: the first one excites the spins, the second  $90^\circ$ -pulse brings the magnetization to the longitudinal  $z$ -direction, and the third pulse brings it back to the transverse  $xy$ -plane. This makes the PGSTE sequence more fit for samples with short  $T_2$ , since the  $z$ -storage prevents transverse relaxation.

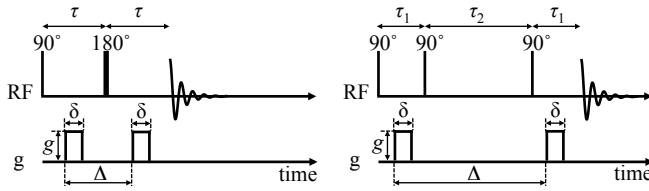


**Figure 3.6:** Two common pulse sequences used to measure diffusion: Pulsed gradient spin echo (PGSE) (left) and pulsed gradient stimulated echo (PGSTE) (right). The upper panel shows the RF-pulses as well as the FID. The lower panel shows the pulsed field gradients with duration,  $\delta$ , gradient pulse spacing  $\Delta$ , and gradient strength,  $g$ . In PGSE, the magnetization is in the transverse plane during the delays  $\tau$ .

In PGSE, the magnetization is in the transverse plane during the whole sequence and echo formation occurs after  $2\tau$ . In the PGSTE sequence, the magnetization is in the transverse plane during the delays  $\tau_1$  and in the longitudinal direction during delay  $\tau_2$ . The echo forms when the second  $\tau_1$  delay ends. The gradient pulses are applied in order to encode for diffusion. They have duration  $\delta$ , strength  $g$  and the spacing between the onset of the gradients is denoted  $\Delta$ . After the excitation pulse, before any gradient is applied and if relaxation is ignored, all spins are precessing with the Larmor frequency and all have the same phase,  $\phi = 0$ . During the application of the first gradient, the precession frequency of the spin will depend on its position along the direction of the applied gradient. The spin will precess faster or slower than  $\omega_0$ , depending on if the field strength it is subjected to, is higher or lower than  $B_0$ . If the short gradient pulse (SGP) approximation is fulfilled, *i.e.* if  $\delta$  is very sharp and diffusion can be ignored during the application of the pulse, then the spin acquires a phase,  $\phi$ , which depends on its position  $\mathbf{r}$ , the gradient duration  $\delta$ , and the gradient strength  $\mathbf{g}$ , according to

$$\phi(\mathbf{r}) = \gamma\delta\mathbf{g} \cdot \mathbf{r}. \quad (3.12)$$

The effect of the gradient on the phase of the spins is commonly quantified by the  $q$ -vector, which is given by<sup>1</sup>

$$\mathbf{q} = \gamma\delta\mathbf{g}. \quad (3.13)$$

In order for the second gradient pulse to rephase the spins it needs to have the opposite

### 3 Nuclear Magnetic Resonance

effect on the phase compared to the first gradient. For the PFG-sequences shown in Fig. 3.6 this is achieved by applying a gradient with the same  $\delta$  and  $g$  in the same direction as the first one, after the magnetization has been inverted. In general, the spins will be rephased when<sup>1</sup>

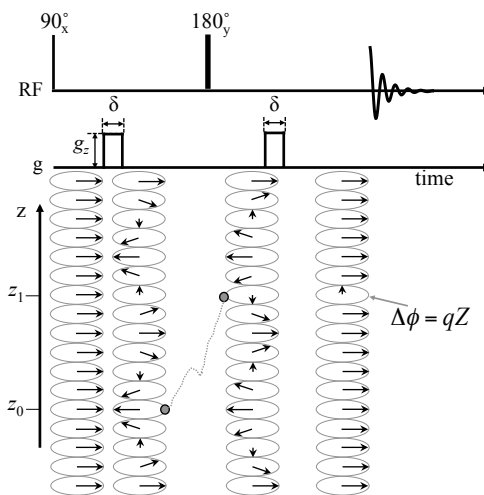
$$\int_0^t \mathbf{g}(t') dt' = 0, \quad (3.14)$$

where  $\mathbf{g}$  is the effective gradient. This also applies for sequences with more complicated gradient shapes than the PFG-sequences. If the spins move during the time between the application of the two gradients, the rephasing of the spins will not be complete. The residual phase of the spin depends on the displacement  $\mathbf{R} = (\mathbf{r}_1 - \mathbf{r}_0)$  during the time between the gradients, and is given by

$$\Delta\phi(\mathbf{r}_1) = \gamma\delta\mathbf{g} \cdot \mathbf{R} \quad (3.15)$$

The effect that the gradients have on the phase, and the effect of the diffusion of one spin can be seen in Fig. 3.7.

**Figure 3.7:** Schematic of how the PGSE sequence effects the phase of the magnetizations. After the  $90^\circ$  pulse, spins are precessing in the transverse plane and the phase is the same everywhere. After applying a gradient pulse in the  $z$ -direction, the phase of the spins will change as a function of position  $z$ . The second gradient pulse has the same duration,  $\delta$ , strength,  $g$ , and direction,  $+z$ , as the first gradient, but since it is applied after the  $180^\circ$ -pulse it will have the opposite effect and rephases the spins. However, a spin that diffuses from position  $z_0$  to  $z_1$ , during the diffusion time, will acquire a residual phase, which depends on the displacement  $Z = (z_1 - z_0)$  and  $q = \gamma\delta g$ .



The total signal from all spins is given by the ensemble average

$$S = \langle \exp(i\phi) \rangle \quad (3.16)$$

and thus, diffusion will cause signal attenuation due to less uniform phase of the spins in the sample. The signal attenuation is given by<sup>34</sup>

$$S/S_0 = \int_{-\infty}^{\infty} P(\mathbf{R}, \Delta) \exp(i\mathbf{q} \cdot \mathbf{R}) d\mathbf{R}, \quad (3.17)$$

which is the Fourier transform of the propagator and where  $S_0$  is the signal in the absence of gradients. For Gaussian diffusion or in the low  $q$ -limit signal attenuation depends on the MSD in one dimension, according to

$$S/S_0 = \exp\left(-\frac{1}{2}q^2 \langle Z^2 \rangle\right). \quad (3.18)$$

and inserting Eq. 2.7 yields

$$S/S_0 = e^{-q^2 D \Delta}. \quad (3.19)$$

In the case of finite gradient pulse widths, the signal attenuation depends on the effective diffusion time  $t_D$ , according to

$$S/S_0 = e^{-bD} \quad (3.20)$$

where  $b = q^2 t_D$  is the diffusion weighting factor, which for the sequences shown in Fig. 3.6, is given by<sup>32</sup>

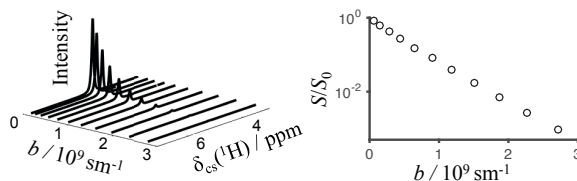
$$b = (\gamma \delta g)^2 (\Delta - \delta/3). \quad (3.21)$$

Experimentally,  $b$  is usually varied by changing the strength,  $g$ , of the pulsed gradients. Fig. 3.8 shows how the intensity of the water peak in a proton spectrum decreases as the diffusion weighting factor,  $b$ , is increased. The signal attenuation,  $S/S_0$ , is mono-exponential as shown in Eq. 3.20, which gives a straight line in a semilogarithmic plot. The diffusion coefficient is calculated by fitting Eq. 3.20 to the data.

For free diffusion Eq. 3.20 is valid for all gradient shapes, but it is not valid when

### 3 Nuclear Magnetic Resonance

**Figure 3.8:** NMR spectra of water shown at different amount of diffusion weighting,  $b$ , calculated according to Eq. 3.21. The normalized signal intensity  $S/S_0$  as a function of  $b$  is plotted in a semilogarithmic plot.



diffusion is restricted. For finite gradient pulses, the spins will have time to diffuse during the application of the pulse and the encoded position will be the center-of-mass of the propagator during the pulse.<sup>35</sup> This fact can be used to measure diffusion coefficient of intracellular water<sup>36</sup>, as well as for pore space imaging.<sup>37;38</sup>

## 3.7 Imaging

In NMR imaging, gradients are used to spatially resolve the NMR signal.<sup>39</sup> In order to get a two dimensional image of the sample, spatially encoding needs to be done in two orthogonal directions. Two different gradients are used during different times of the pulse sequence, which often is a spin echo sequence. One of the gradients is the frequency encoding gradient  $G_f$ , which is applied during signal acquisition. The phase encoding gradient  $G_p$ , is applied before signal acquisition. The gradients define a reciprocal space, also called  $k$ -space, according to

$$\mathbf{k} = \int \mathbf{G}(t) dt. \quad (3.22)$$

By doing a 2D Fourier transform of  $k$ -space a 2D-image of the studied object is generated, with each pixel intensity in the image correspond to the NMR signal acquired at a specific position in the studied object. By exciting one slice at a time a 3D reconstruction of the object can be obtained. Each volumetric picture element is called a voxel.

### 3.7.1 Diffusion tensor imaging

For some heterogenous system such as biological tissue or liquid crystal (see Section 4.1.1), anisotropy of the microscopic structures in the sample can give anisotropic diffusion. The signal attenuation will depend on the distribution of apparent diffusivities in



the sample, which will be discussed in more detail in Chapter 5.

Diffusion can be described with the diffusion tensor given in Eq. 2.10. By repeating diffusion encoding measurements in several non-collinear directions it is possible to compute the diffusion tensor of each voxel. This technique is called diffusion tensor imaging (DTI).<sup>18</sup> A common parameter used to describe the amount of anisotropy of each voxel is the fractional anisotropy (FA). FA is calculated from the eigenvalues of principal coordinate axis diffusion tensor and the mean diffusivity  $\bar{D}$ , according to<sup>31</sup>

$$FA = \sqrt{\frac{3}{2}} \sqrt{\frac{(\lambda_1 - \bar{D})^2 + (\lambda_2 - \bar{D})^2 + (\lambda_3 - \bar{D})^2}{\lambda_1^2 + \lambda_2^2 + \lambda_3^2}}. \quad (3.23)$$

Some other parameters, useful to describe the diffusion tensor is the parallel diffusion coefficient,  $D_{\parallel}$ , and the perpendicular diffusion coefficient,  $D_{\perp}$ . If the diffusion tensor has a prolate shape then  $D_{\parallel} > D_{\perp}$  and if the diffusion tensor has an oblate shape then  $D_{\parallel} < D_{\perp}$ .

One problem with DTI is that it only reflects the macroscopic diffusion anisotropy in a voxel and does not reflect the microscopic anisotropic diffusion inside the anisotropic pores in the sample. In Fig. 3.9 three voxels containing the same type of microscopic pore shapes, cylinders in this case, are shown. The macroscopic diffusion tensor of each voxel is shown, and it is clear that the diffusion tensor does not correspond to the underlying microscopic structure but rather affected by the orientation distribution of the microscopic domains.

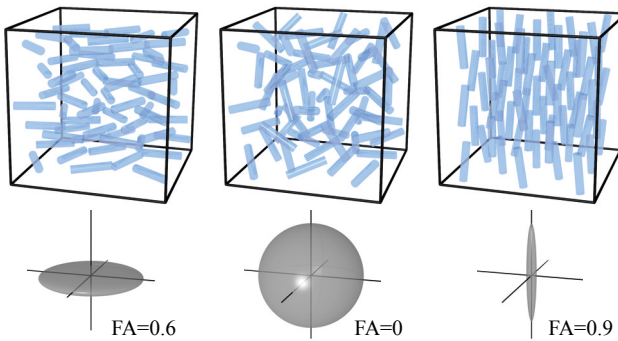


**Figure 3.9:** Three different voxels with the same microscopically anisotropic structure but with different orientation distributions. The ordering of the cylinders reflect the shape of the diffusion tensor and the FA calculated according to Eq. 3.23.



# 4

## Colloidal model systems

A colloidal system is defined as a macroscopically homogeneous sample containing nano- to micrometer sized particles or assemblies that are evenly suspended in another type of material. Some examples are: oil droplets dispersed in water, dust particles distributed in air, and blood cells suspended in blood plasma.

Some particles, such as surfactants, which can be suspended in water, have the ability to self-assemble into a range of organized colloidal structures.<sup>13</sup> Consequently, the water is constrained by the aggregates and will in some structures diffuse anisotropically. Anisotropic water diffusion can also be found in biological tissues such as in white brain matter. For this reason we have chosen to use surfactant based systems to model anisotropic diffusion of biological tissues.

Another system, which has shown to be useful as a model system in NMR diffusion studies, is yeast cell suspensions.<sup>36</sup> Yeast cells can also be used as a biological model organism, since it can be genetically modified to express human proteins.<sup>40</sup> In this chapter, some aspects of the different model systems used in this thesis will be explained in more detail.

### 4.1 Surfactants

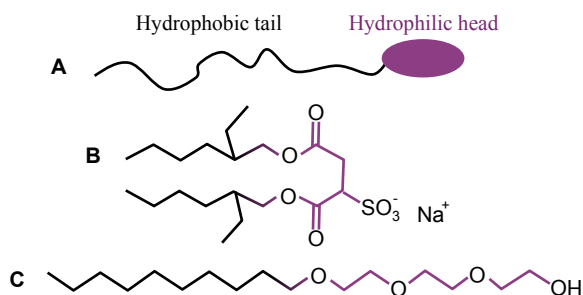
Surfactants are amphiphilic molecules, which consist of two parts: one part which is soluble in water, the hydrophilic head, and one part which is not soluble in water, the hydrophobic tail. These type of molecules are common in everyday life, in products such as shampoo and toothpaste, as well as in many other applications, *e.g.* enhancing

## 4 Colloidal model systems

oil recovery and facilitating drug administration.<sup>41</sup> The name surfactant comes from the fact that they are active at surfaces and can decrease the surface tension between different phases.<sup>13;41</sup>

There are many types of surfactants with different characteristics. Depending on the charge of the headgroup, the surfactant can be either, anionic (negatively charged), cationic (positively charged), zwitterionic (both positively and negatively charged) or nonionic (not charged). The charge of the head group will play an important role for the type of aggregates that are formed as the surfactants self-assemble. In Fig. 4.1 a typical surfactant is illustrated with a hydrophobic tail and a hydrophilic head. The chemical structure of two different surfactants is also shown: AOT, which is anionic and the  $C_{10}E_3$ , which is nonionic.

**Figure 4.1:** (A) Schematic figure of a surfactant with a hydrophilic head and a hydrophobic tail. (B) The chemical structure of the sodium 1,4-bis(2-ethyl-hexyl) sulfosuccinate (AOT), which was used in Papers I and III. (C) Triethylene glycol monodecyl ether ( $C_{10}E_3$ ) was used in Paper. II.



The simplest type of self-assembled aggregate that surfactants can form is a spherical micelle, in which the hydrophobic tails from numerous surfactants merge together and form a sphere-like particle with the polar heads pointing out towards the solution. This will effectively separate the non-polar tails from the water, which is energetically favourable.<sup>13</sup>

Depending on the effective area of the polar head and the length and volume of the hydrocarbon tail the shape of the self-assembled structures can take many different forms.<sup>42</sup> Also the concentration of surfactants in solution will influence the aggregate structure, as well as, pH, salt concentration and temperature.<sup>13</sup> In Fig 4.2 different types of aggregate structures are shown. The polar heads always points towards the water phase and the apolar hydrocarbon tails merge and create a continuous nonpolar phase.

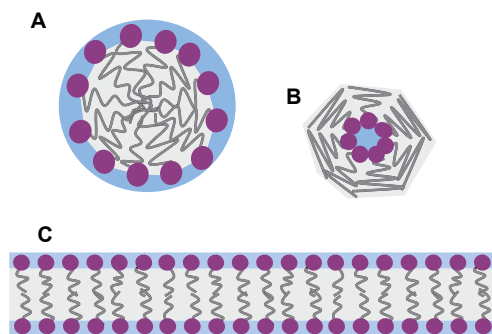


**Figure 4.2:** Schematic representations of some self-assembly structures created by surfactants in aqueous solution. (A) Normal micelle, where the polar heads point outwards into the water and the apolar hydrocarbon tails point inward, creating a nonpolar region in the micellar core. (B) Reverse micelle, where the water constitutes the core of the micelle. (C) Surfactant bilayer consisting of two surfactant mono-layers where the apolar hydrocarbon tails create the core.

### 4.1.1 Lyotropic liquid crystals

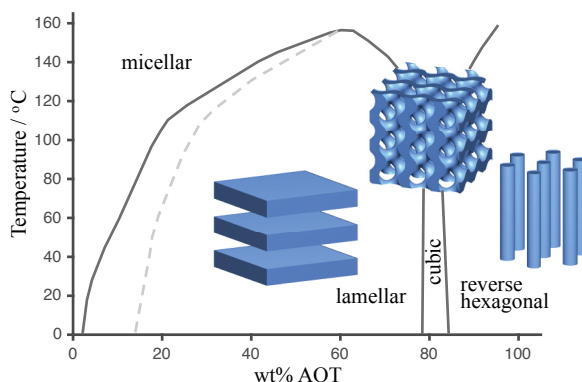
It is normal for surfactants in water solution to form lyotropic liquid crystals.<sup>43</sup> These crystalline structures are microscopically ordered and they are liquid in the sense that there is a high molecular mobility. Three different classes of liquid crystalline phases are: lamellar, cubic and hexagonal. In Fig. 4.3 the water phase in the three classes are depicted. The lamellar and the hexagonal phases have anisotropic water diffusion while the cubic phase is isotropic. The lamellar phase consists of stacks of surfactant bilayers separated by water, which can diffuse freely in the plane perpendicular to the symmetry axis of the domain but is restricted in the parallel direction. The hexagonal phase consists of stacks of rod-shaped micelles, normal or reversed, packed in a hexagonal pattern. In the reversed hexagonal phase (shown in Fig. 4.3) the water diffuses freely along the symmetry axis but is restricted in the perpendicular direction. A bicontinuous cubic phase show isotropic diffusion for both the water and the surfactant.

The phase of the liquid crystal is highly dependent on the type of surfactant as well as on the concentration of the surfactant in solution and the temperature. A phase diagram shows under which conditions the various phases are thermodynamically stable.

In Fig. 4.3, the AOT/water phase diagram<sup>44</sup> shows the phases at different concentrations and temperatures. There are three areas that generates lyotropic liquid crystals, a big area with lamellar phase at intermediate concentrations, a small range with a bicontinuous cubic phase and reverse hexagonal phase at high concentrations.

## 4 Colloidal model systems

**Figure 4.3:** Phase diagram for an AOT/water solution. Three areas with different liquid crystal structures can be seen: Lamellar at intermediate concentrations, cubic around 80 wt% AOT, and reverse hexagonal at high concentrations. The blue colour shows the water compartment geometries of the different phases.



## 4.2 Characterizations of liquid crystals

### 4.2.1 SAXS

A common technique used to study the structure of liquid crystals is small angle X-ray scattering (SAXS). In SAXS the sample is irradiated with X-rays with a certain wavelength  $\lambda$ . Most of the photons will go through the sample without any interaction but some of the photons will scatter elastically as they hit an electron. The scattered light will be detected at a range of small angles  $\theta$ , from the incidence point of the primary beam. If there is an ordered structure in the sample, constructive interference will occur at  $\theta$ , according to Bragg's law<sup>13</sup>

$$n\lambda = 2d\sin\theta, \quad (4.1)$$

where  $n$  is an integer and  $d$  is the repeating distance between the scattering elements.

The diffraction pattern from the scattered photons can give information about the liquid crystal structure of the sample and it is possible to see whether the structure is lamellar, cubic or hexagonal.<sup>45</sup>

### 4.2.2 $^2\text{H}$ NMR

If a liquid crystal contains heavy water,  $\text{D}_2\text{O}$ ,  $^2\text{H}$  NMR can be used to determine if the system is anisotropic. Because the  $^2\text{H}$  nuclei has spin quantum number,  $I = 1$ , it

possesses a quadrupolar moment, which changes the energy levels of the  $^2\text{H}$  nucleus slightly so that they become non-equidistant.<sup>27</sup> This can cause a splitting in the NMR spectrum. The amount of splitting depends on the water molecule's orientation relative to the main magnetic field,  $B_0$ . However, no splitting will occur when the water is moving isotropically, as in *e.g.* free water, because then the affect of the quadrupolar interaction will average out. In anisotropic samples on the other hand, such as in lamellar or hexagonal liquid crystals, the water positioned closest to the surfactants will have a preferred orientation, because of the interaction with the polar head group. The size of the splitting will depend on the orientation of the liquid crystal structure, relative to  $B_0$ .<sup>46</sup> If the sample is completely ordered and there is only one orientation of the crystalline structures, two peaks will appear in the spectrum. If the orientations of the crystalline structures is isotropic, *i.e.* all orientations occur with the same probability, the NMR peak will take the form of a Pake pattern,<sup>47</sup> with contributions from all different orientation, where  $0^\circ$  is the least probable angle, relative to  $B_0$ , and  $90^\circ$  is the most probable angle.<sup>46</sup> In cubic phased liquid crystals, where the surfactant layer has no preferred direction, no splitting will occur.

### 4.3 Yeast cells

Yeast cells were used early as a model system by Stejskal and Tanner<sup>15</sup> to show the effect of restricted diffusion for PFG-experiments. Since then the system has been used in many studies with diffusion NMR.<sup>36;48-51</sup> Yeast cells are eukaryotic unicellular organisms and they have many similarities to human cells, but they can grow much faster.<sup>52</sup>

One important component of the cell is the cell membrane. The cell membrane consists of a phospholipid bilayer and constitutes a barrier for molecular diffusion processes.<sup>13</sup> The membrane also contains different types of proteins with different functions.

Yeast is also popular as a model in biological studies. Baker's yeast, (*Saccharomyces cerevisiae*) was the first eukaryotic cell to have its entire genome completely sequenced.<sup>53</sup> Since then, different types of yeast cell strains has been used to study and understand human biological processes. For example, yeast cells can be genetically modified to

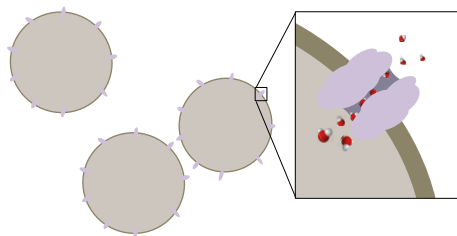
express human proteins such as aquaporins.

### 4.3.1 Aquaporins

Water transport across the biological cell membranes are of great importance for the functionality of cells. There are different mechanisms behind this process,<sup>54</sup> one of them is passive water transport through special membrane proteins called aquaporins (AQP).

There are many different types of human AQP and they are found at different locations in the body.<sup>55;56</sup> AQP has shown to play a role in several diseases, including different type of cancers.<sup>57</sup> Better understanding of the mechanisms of the AQP may contribute to new types of diagnostics and therapeutics.<sup>56;57</sup> An illustration of yeast cells with aquaporins expressed in the cell membrane is shown in Fig. 4.4.

**Figure 4.4:** Illustration of yeast cells with aquaporins in the cell membrane. The aquaporin is a transport protein, which passively lets water in and out of the cell.





# 5

## Diffusion NMR for microscopic anisotropy

As we have seen in previous chapters, the mean square displacement of a spin ensemble can be affected by restrictions preventing further displacement in that direction, which in turn affects the ADC. If diffusion is measured in several directions the diffusion tensor can be retrieved. However, the diffusion tensor reflects the anisotropy on a macroscopic scale. If the domains in the sample are randomly oriented, the resulting diffusion tensor will be isotropic. In Papers I-III we introduce methods that go below voxel level and quantify the microscopic anisotropy. The shape of the microscopic anisotropic diffusion tensor can also be determined.

In this chapter, diffusion NMR in anisotropic structures will be explored and the novel methods developed in paper I-III will be summarized.

### 5.1 Conventional diffusion encoding

For free diffusion signal attenuation will follow Eq. 3.20, and the measured diffusion coefficient corresponds to the self-diffusion coefficient of the molecule. For restricted diffusion the signal attenuation will depend on the size and shape of the compartment and the diffusion time.

Consider a cylinder shaped compartment with water inside the cylinder and no water outside the cylinder. The diffusion parallel to the axis of the cylinder,  $D_{\parallel}$ , will be free and non-restricted while the diffusion perpendicular to the cylinder,  $D_{\perp}$  will be restricted. In Fig. 5.1 it is shown how the apparent diffusion coefficient measured by conventional diffusion NMR depends on the angle  $\theta$ , between the encoded diffusion direction (the

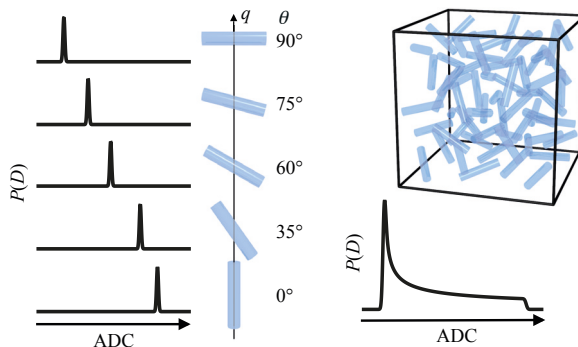
## 5 Diffusion NMR for microscopic anisotropy

$q$ -vector) and the cylindric compartment. If there is only one cylinder or if all cylinders inside the studied volume are ordered with the same direction the signal acquired with a conventional diffusion NMR experiment follows a mono-exponential decay (see Fig. 3.8) with the steepest slope at  $\theta = 0^\circ$  and the most flat slope at  $\theta = 90^\circ$ . The apparent diffusion coefficient at a specific angle is given by<sup>4</sup>

$$D_\theta = D_{\parallel} \cos^2 \theta + D_{\perp} \sin^2 \theta \quad (5.1)$$

The probability of a certain apparent diffusion coefficient,  $P(D)$ , is in this case a delta function. However, if the volume contains randomly oriented cylinders the distribution of apparent diffusion coefficients forms half a Pake pattern, with a high probability of low ADCs and a low probability of high ADCs.

**Figure 5.1:** The apparent diffusion coefficient, ADC, measured in anisotropic materials depends on the angle of the  $q$ -vector in relation to the anisotropic structure. For a sample with randomly distributed orientations the probability distribution will follow half a Pake pattern (bottom right).



The signal attenuation curve from a sample like the one shown in Fig. 5.1 is multi-exponential, composed of all the ADC coefficients from the cylinders with different orientations, according to

$$S/S_0 = \int_0^{\infty} P(D) e^{-bD}. \quad (5.2)$$

The curvature of the signal attenuation has previously been used to distinguish between different phases in AOT liquid crystals,<sup>2</sup> and the shape of  $P(D)$  can be used to describe diffusion in cellulose and starch.<sup>4</sup> In Fig. 5.2 the signal attenuation curves for lamellar and reverse hexagonal liquid crystals are shown.

It should be noted that the curved signal attenuations like those shown in Fig. 5.2 and

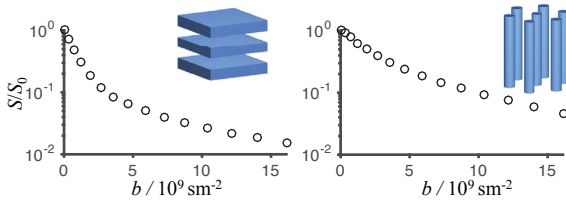


**Figure 5.2:** Signal attenuation resulting from conventional diffusion encoding on a lamellar liquid crystal (left) and a reverse hexagonal liquid crystal (right).

the probability distribution of diffusion coefficients of the type shown in Fig. 5.1 are not specific for anisotropic diffusion. The exact same probability distribution could be generated by a collection of spherical pores of different sizes, contributing to different ADCs with the same probability as in Fig. 5.1. This ambiguity can be solved by using more advanced pulse sequences.

## 5.2 More encoding directions

If we move beyond the conventional diffusion encoding sequences *e.g.* PGSE and PGSTE, the diffusion encoding sequence can be extended and encode more than one direction. This was done by Callaghan and Komlosh<sup>20</sup> when they applied a double diffusion encoding sequence to an AOT-water lamellar liquid crystal and combined encodings with collinear and orthogonal gradient directions in order to distinguish between isotropic and anisotropic diffusion on the microscopic scale. The same approach was used in a study of diffusional anisotropy in the spinal cord.<sup>58</sup> It is also possible to study the full angular dependence between the two encoding directions by varying the angle, stepwise, from  $0^\circ$  to  $360^\circ$ .<sup>59–61</sup>

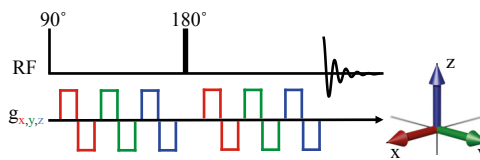
## 5.3 Isotropic diffusion encoding

For anisotropic diffusion tensors the mean diffusion,  $\overline{D}$ , (see Eq. 2.11) is invariant of the direction of the principal frame of the anisotropic compartment. It is possible to measure the trace of the diffusion by encoding for three orthogonal diffusion directions within the same pulse sequence.

A simple way to do this is to use bipolar gradients in three orthogonal directions, for

example  $x, y$  and  $z$ , on each side of the  $180^\circ$  pulse in a normal spin echo.<sup>62</sup> A schematic of the sequence as well as the corresponding vector directions are shown in Fig. ref:tripleIso. The diffusion encoding vectors are built up and down for each bipolar gradient pulse. For this particular sequence the encoding vector will be built up six times during the pulse sequence. Combinations of more than one gradient direction at once can also be used in order to increase the maximum gradient power.<sup>62,63</sup> The combination of encoded directions must be done in such a way that the off-diagonal elements of the diffusion tensor are cancelled out. More RF-pulses during the sequence can also be applied.<sup>63,64</sup>

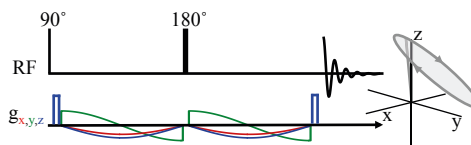
**Figure 5.3:** Isotropic diffusion weighting with three orthogonal bipolar gradient pulses on each side of the  $180^\circ$  pulse. The different colours show the different gradient directions  $x$  (red),  $y$  (green) and  $z$  (blue). The arrows are the corresponding diffusion encoding vectors.



### 5.4 $q$ -MAS - magic angle spinning of the $q$ -vector

In Paper I, we introduce a novel sequence, which instead of pulsing the diffusion encoding vector in several separate directions, builds up the diffusion encoding vector once and then, by using harmonically modulated gradients in the  $x, y$  and  $z$ -directions, continuously changes the azimuth angle,  $\psi$ , of the  $q$ -vector, keeping it at a constant inclination angle,  $\zeta = \arccos(1/\sqrt{3}) \approx 54.7^\circ$ , also called the 'magic angle'.<sup>65</sup>

**Figure 5.4:** A schematic of the  $q$ -MAS pulse sequence. The  $q$ -vector is built up by the  $z$ -gradient and modulations of the  $x, y$  and  $z$  gradients cause the vector to rotate one lap at the magic angle.



The resulting signal attenuation from an isotropic diffusion encoding, reveals the mean diffusion of the microscopic diffusion tensor, and the anisotropic contribution to the signal attenuation will vanish. This can be seen clearly in Fig. 5.5 where the signal attenuation from three different samples are shown: lamellar liquid crystal, reverse hexagonal

## 5.5 Quantifying microscopic anisotropy with isotropic diffusion weighting

and yeast cell suspension. Corresponding  $P(D)$ s are shown next to the signal attenuation plots. The signal attenuation from the conventional diffusion encoding sequence is plotted in blue, the signal attenuation from isotropic diffusion weighting is plotted in red. The isotropic diffusion weighting shows a mono-exponential decay for the lamellar and the reverse hexagonal liquid crystal, and their  $P(D)$ s show the mean diffusivity. The signal attenuation from the yeast cell suspension on the other hand, shows the same signal attenuation for both conventional and isotropic diffusion weighting. This is because the cells are spherical and therefore diffusion is isotropic.

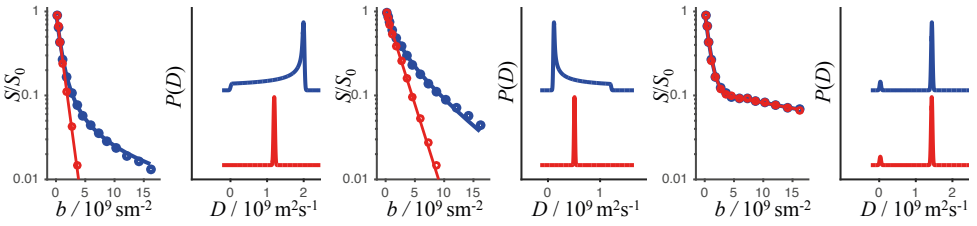


**Figure 5.5:** Signal attenuation for conventional diffusion encoding (blue) and isotropic diffusion encoding (red) for three different samples: Lamellar liquid crystal (left), reverse hexagonal (middle) and yeast cell suspension (right). The corresponding probability distribution of apparent diffusion coefficients,  $P(D)$ , are plotted next to the signal attenuation curves.

## 5.5 Quantifying microscopic anisotropy with isotropic diffusion weighting

In Paper II we implement a  $q$ -MAS sequence with smooth gradient modulations, which are less demanding for the gradients and thus better suited for a clinical system.<sup>66</sup> The sequence is shown in Fig. 5.6.

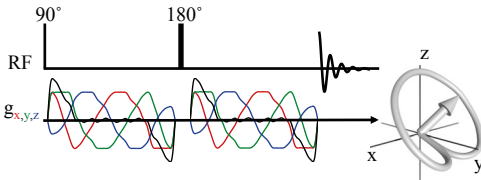


**Figure 5.6:**  $q$ -MAS with smooth modulated gradients  $x$ ,  $y$  and  $z$  are shown in red, green and blue, respectively. The corresponding  $q$ -vector trajectory is shown. The black line shows the gradient shape used for the conventional diffusion encoding.

## 5 Diffusion NMR for microscopic anisotropy

---

To quantify the microscopic anisotropy we use the fact that the variance,  $\mu_2$ , of  $P(D)$  (also called the second central moment) corresponds to the first deviation from a mono-exponential attenuation curve. Also the  $\mu_2$  observed from a sample with randomly ordered domains, correspond to the microscopic anisotropic diffusion inside the compartments. This can be seen in Fig. 5.1 where the  $P(D)$  is achieved by a completely random orientation of microscopically anisotropic domains, shaped like cylinders in this case. However, if the order of domains is higher on a macroscopic scale, the  $P(D)$  will not look the same. We can simulate completely random orientations by applying powder averaging, which will be explained below.

The amount of ordering in a sample can be quantified with the order parameter,

$$\text{OP} = \langle (3\cos^2\varphi - 1)/2 \rangle, \quad (5.3)$$

where  $\varphi$  is the angle between the principal axis of the anisotropic domain and the voxel symmetry axis. The values for OP can be between -1/2 and 1. In Fig. 5.1 the orientations of the compartments are completely random, giving  $\text{OP} = 0$ . If  $\text{OP} > 0$  then  $P(D)$  will not have the same shape any more. This means that the  $\mu_2$  of  $P(D)$  will not reflect the diffusion tensor of the microscopically anisotropic compartments.

Powder averaging can be done by acquiring the conventional diffusion encoding signal with many orientations, uniformly distributed on a unit sphere<sup>67;68</sup> and averaging the signal. The resulting signal attenuation will correspond to a sample with randomly oriented domains,  $\text{OP} = 0$ .

The difference in variance of the  $P(D)$ s, resulting from powdered average diffusion encoding and isotropic encoding, is given by

$$\Delta\tilde{\mu}_2 = \frac{\mu_2 - \mu_2^{\text{iso}}}{\bar{D}^2}, \quad (5.4)$$

where  $\mu_2$  is the variance of the powder averaged conventional diffusion encoding and  $\mu_2^{\text{iso}}$  is the variance of the isotropic diffusion encoding.

The microscopical fractional anisotropy,  $\mu\text{FA}$ , is defined as

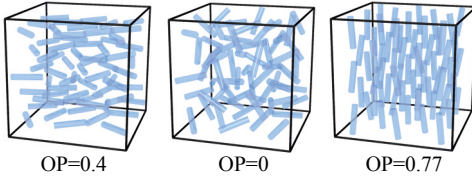
$$\mu\text{FA} = \sqrt{\frac{3}{2}} \left( 1 + \frac{2}{5} \cdot \frac{1}{\Delta\tilde{\mu}_2} \right)^{-1/2} \quad (5.5)$$

## 5.5 Quantifying microscopic anisotropy with isotropic diffusion weighting

and describes the anisotropic diffusion inside the microscopic domains.  $\mu_{FA}$  is the microscopic equivalent of FA (see Eq. 3.23). OP can be calculated from  $\mu_{FA}$  and FA in the following way

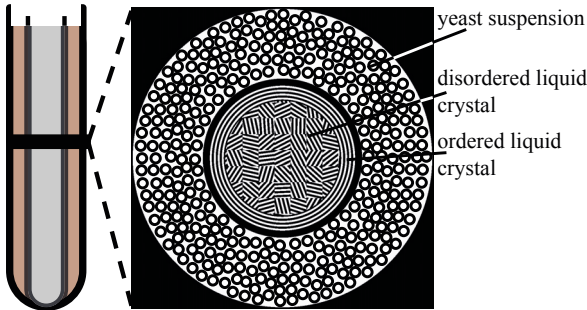
$$OP = \sqrt{\frac{3\mu_{FA}^{-2} - 2}{3FA^{-2} - 2}}. \quad (5.6)$$

Fig. 5.7 show three voxels with the same  $\mu_{FA}$  but with different OP.



**Figure 5.7:** Three voxels showing different order parameter, OP. The microscopic fractional anisotropy,  $\mu_{FA}$ , are the same in all voxels but the orientations of the cylinders are different. OP was calculated with Eq. 5.6 assuming,  $\mu_{FA}=1$  and FA values of: 0.6, 0 and 0.9, respectively.

Fig. 5.8 shows an MRI phantom that can be used for imaging microscopic anisotropy. The phantom contains anisotropic diffusion in a  $C_{10}E_3$ -water lamellar liquid crystal and isotropic diffusion in a yeast cell suspension.



**Figure 5.8:** Schematic illustration of an MRI phantom for microscopic anisotropy. The phantom consists of two different sized NMR tubes. The inner tube contains a  $C_{10}E_3$ -water lamellar liquid crystal, which is ordered at the edge and random in the middle. The outer tube contains a yeast cell suspension.

By acquiring the signal with an imaging sequence, it is possible to study the signal attenuation of each voxel. In Fig. 5.9, four voxels from the MRI phantom is shown. Isotropic diffusion weighting causes variance  $\mu_2^{\text{iso}} = 0$  in the ordered and the disordered liquid crystal. In the yeast cell suspension  $\mu_2^{\text{iso}} = \mu_2$ , since the diffusion is isotropic. If both yeast and liquid crystal are present in the same voxel, the isotropic diffusion encoding removes the contribution from anisotropic diffusion but  $\mu_2^{\text{iso}} > 0$ , because of the different diffusivities in the yeast suspension.

## 5 Diffusion NMR for microscopic anisotropy

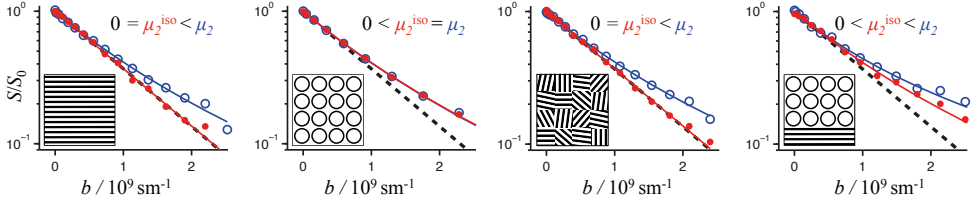
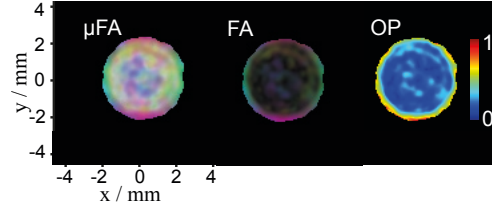


**Figure 5.9:** Signal attenuation plots from conventional diffusion weighting (blue) and isotropic diffusion weighting (red) for different sites in the MRI phantom. The plots shown from left to right correspond to: ordered lamellar liquid crystal; yeast cell suspension; randomly ordered liquid crystal; mixture of liquid crystal and yeast cell suspension. The relations between  $\mu_2$  and  $\mu_2^{iso}$  are shown for each situation.

The parameters  $\mu FA$ , FA and OP of the anisotropic diffusion in the liquid crystal can be quantified from the signal attenuation curves and mapped, as shown in Fig. 5.10. The  $\mu FA$  map show high intensity everywhere in the liquid crystal, FA is only high at the outer edge of the inner tube. OP looks similar to FA, with high intensity at the outer edge of the inner tube and low intensity in the middle, which follows Eq. 5.6.

**Figure 5.10:** Three MR-images of the phantom shown in Fig. 5.8. The three parameters: microscopic fractional anisotropy,  $\mu FA$ , fractional anisotropy, FA, and order parameter, OP, are mapped. The colours in the FA map correspond to the  $xx$  (red),  $yy$  (green),  $zz$  (blue) elements in the laboratory-frame diffusion tensor. The colours in the OP map go from blue = 0 to red = 1. In these images the yeast has been cut out.



### 5.6 Prolate or oblate?

In Paper III the shape of the microscopic diffusion tensor is quantified.

The diffusion tensor  $\mathbf{D}$  can be diagonalized to its principle axis system and parametrized into its isotropic value  $D_{iso}$ , (mean diffusion as shown in 2.11), its anisotropy,  $D_{\Delta}$ , and its asymmetry  $D_{\eta}$ . The  $D_{\Delta}$  and  $D_{\eta}$  of  $\mathbf{D}$  is given by

$$D_{\Delta} = \frac{1}{3D} \left( D_{zz} - \frac{D_{yy} + D_{xx}}{2} \right) \quad (5.7)$$



and

$$D_\eta = \frac{D_{yy} - D_{xx}}{2D_{\text{iso}}D_\Delta} \quad (5.8)$$

The diagonal elements are order according to the convention  $|D_{zz} - D_{\text{iso}}| \geq |D_{xx} - D_{\text{iso}}| \geq |D_{yy} - D_{\text{iso}}|$ . For axially symmetric diffusion,  $D_\eta = 0$ . Positive and negative values of  $D_\Delta$  correspond to prolate and oblate shapes, respectively.

Diffusion weighting can be described by the diffusion-weighting matrix  $\mathbf{b}$ :<sup>1;29</sup>

$$\mathbf{b} = \begin{pmatrix} b_{xx} & b_{xy} & b_{xz} \\ b_{yx} & b_{yy} & b_{yz} \\ b_{zx} & b_{zy} & b_{zz} \end{pmatrix}. \quad (5.9)$$

For axially symmetric diffusion encoding,  $\mathbf{b}$  can be parametrized into its trace  $b$ , and anisotropy  $b_\Delta$ :

$$b = \text{Tr}(\mathbf{b}) = b_{xx} + b_{yy} + b_{zz} \quad (5.10)$$

and

$$b_\Delta = \frac{1}{b} \left( b_{zz} - \frac{b_{yy}}{b_{xx}} \right). \quad (5.11)$$

The diffusion-weighting is isotropic if  $b_{xx} = b_{yy} = b_{zz} = \text{Tr}(\mathbf{b})/3$  and results in no anisotropy of the diffusion-weighting,  $b_\Delta = 0$ . The diffusion encoding is done by using the triple-stimulated echo sequence<sup>69</sup> shown in Fig. 5.11.

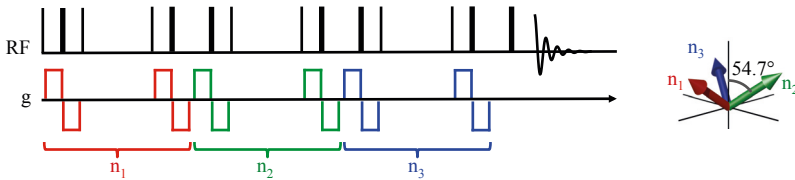
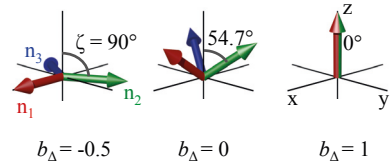


**Figure 5.11:** Triple stimulated echo with bipolar gradients. The three  $q$ -vectors, with orientations,  $n_1$ ,  $n_2$  and  $n_3$  are built up and down with bipolar gradient pairs shown in red, green and blue respectively. The inclination angle,  $\zeta$ , is varied to achieve different anisotropy of the diffusion-weighting,  $b_\Delta$ .

## 5 Diffusion NMR for microscopic anisotropy

To achieve isotropic diffusion weighting the inclination angle is  $\zeta = 54.7^\circ$  and the azimuth angles between the vectors are  $120^\circ$ . To change  $b_\Delta$  the angle  $\zeta$  is changed.  $b_\Delta$  can range from -0.5 when  $\zeta = 90^\circ$  to 1 when  $\zeta = 0^\circ$ .

**Figure 5.12:** Axially symmetric diffusion encoding. The inclination angle of the  $q$ -vector is varied to achieve different anisotropies of the diffusion-weighting,  $b_\Delta$ .



The curvature of the signal attenuation curve will depend on  $b_\Delta$ . At  $b_\Delta = 1$  (conventional diffusion encoding) anisotropic diffusion will result in the most curved signal attenuation.  $b_\Delta = 0$ , anisotropic diffusion will give no curvature to the signal attenuation.

By varying  $b$  and  $b_\Delta$  the resulting shape of the signal attenuation will reflect  $D_\Delta$  of the microscopic compartments.

Lamellar, cubic and reverse hexagonal AOT-water liquid crystals were used for proof-of-concept. In Fig. 5.13 the two dimensional attenuation curves are shown as a function of  $b$  and  $b_\Delta$  as well as the corresponding shape of the diffusion tensor.

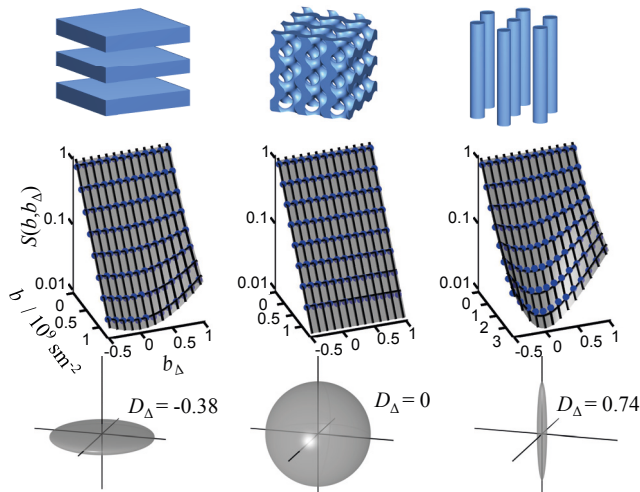


**Figure 5.13:** Two dimensional signal attenuation curves shown for three different structures of liquid crystals: lamellar (left), cubic (middle) and reverse hexagonal (right). The shape of the attenuation curve,  $S(b, b_\Delta)$  is given by the microscopic diffusion anisotropy,  $D_\Delta$ .

# 6

## Diffusion NMR for exchange

The study of transport between different compartments in heterogeneous systems is of interest in many fields. For example, to investigate the functionality of different types of transport proteins in cell membranes, such as aquaporins. The most common way to study exchange in cells is to change the osmolality of the solution<sup>10;70</sup> and to observe the change in cell size. A more direct method for measuring exchange is NMR, since it allows probing the water molecules directly without any osmotic gradient. One way, in which NMR can be used, is to add some type of relaxation agent that will affect the  $T_1$  or  $T_2$  relaxation of the water.<sup>71-73</sup> However, this includes the introduction of a foreign substance and is not always possible. However, using magnetic field gradients to probe the exchange of water molecules between compartments, is a completely non-invasive method.

### 6.1 Conventional diffusion encoding in a two-compartment system

If there is no exchange between two compartment with two different diffusion coefficient, signal attenuation will depend on the fraction and the diffusion coefficient of each compartment,

$$S/S_0 = f_1 e^{-bD_1} + f_2 e^{-bD_2} \quad (6.1)$$

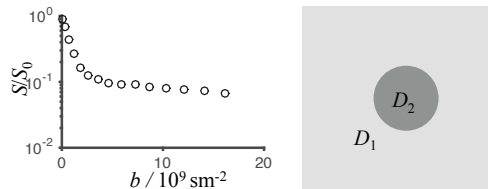
where  $f_1$  and  $f_2$  are the fractions of respective compartment.

## 6 Diffusion NMR for exchange

For a system where one compartment contains freely diffusing molecules and the other contains restricted molecules, as for intra- and extracellular water in a cell suspension, the ADC of each compartment will depend on the diffusion time.<sup>74</sup> If the diffusion time is long enough for the intracellular water displacement to be affected by the restriction, the signal attenuation will be bi-exponential even if the water in both compartments has the same self-diffusion coefficient.

In Fig. 6.1 the bi-exponential signal attenuation of a yeast cell suspension is shown. The intracellular water has a lower ADC,  $D_2 < D_1$ . The signal fraction of the intracellular compartment,  $f_1$ , can be calculated by extrapolating the curve at high  $b$ -values back to  $b = 0$ . The extracellular fraction,  $f_2 = 1 - f_1$ , and the initial slope gives the average diffusion coefficient in the system.

**Figure 6.1:** Signal attenuation for a two compartment system with fast apparent diffusion coefficient,  $D_1$ , in the extracellular water and slower apparent diffusion coefficient,  $D_2$ , in the intracellular space.



If there is exchange between the two compartments, the signal attenuation curve will be affected by the exchange rate.

## 6.2 Methods to study exchange with diffusion NMR

### 6.2.1 Kärger model

The Kärger model<sup>75</sup> can be used to estimate the exchange between two compartments with different diffusion coefficients. The Kärger model has been used for many applications *e.g.* surfactants and polymers in exchange between adsorbed and solvated state<sup>21</sup> as well as permeability of many different types of cell types,<sup>76–78</sup> including yeast cells.<sup>50;79</sup>

The Kärger model is based on the fact that when there is exchange between two compartments with different diffusion coefficients, the signal attenuation of each compartment will include the loss of signal of molecules leaving the compartment, as well as the gain in signal from molecules entering the compartment.<sup>80</sup>

## 6.2 Methods to study exchange with diffusion NMR

---

The signal attenuation for a system with two compartments with different apparent diffusion coefficients,  $D_{1,2}$  and average residence time in each compartment,  $\tau_{1,2}$ , is given by

$$E(q, t_D) = C_A e^{-q^2 D_A t_D} + C_B e^{-q^2 D_B t_D} \quad (6.2)$$

where

$$D_{A,B} = \frac{1}{2} \left\{ D_1 + D_2 + \frac{1}{q^2} \left( \frac{1}{\tau_1} + \frac{1}{\tau_2} \right) \mp \sqrt{\left[ D_1 - D_2 + \frac{1}{q^2} \left( \frac{1}{\tau_1} + \frac{1}{\tau_2} \right) \right]^2 + \frac{4}{q^4 \tau_1 \tau_2}} \right\}, \quad (6.3)$$

$$C_B = \frac{f_1 D_1 + f_2 D_2 - D_A}{D_B - D_A} \quad (6.4)$$

and

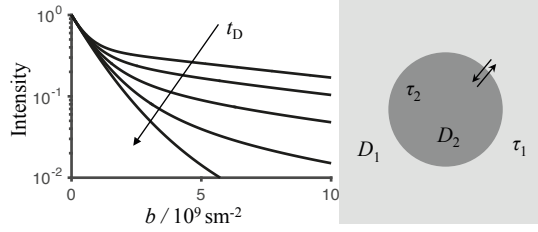
$$C_A = 1 - C_B. \quad (6.5)$$

The typical pulse sequence of a Kärger experiment is a conventional diffusion encoding sequence such as PGSE or PGSTE. By increasing the diffusion time, the signal attenuation will be more affected by exchange. Signal attenuation for a non-restricted system is calculated from the Kärger model and shown in Fig. 6.2. The diffusion coefficients of the different compartments are  $D_1 = 2 \cdot 10^{-9} \text{ ms}^{-2}$  and  $D_2 = 8 \cdot 10^{-11} \text{ ms}^{-2}$ . Here  $t_D$  is increased from 1 ms to 1 s. The fraction of each compartment are  $f_1 = 0.6$  and  $f_2 = 0.4$  and the exchange rate is  $k = 10.4 \text{ s}^{-1}$ . As  $t_D \rightarrow \infty$  the signal attenuation curves becomes mono-exponential corresponding to the mean attenuation of the system, because the diffusing molecules can probe both compartments during the diffusion time.<sup>77</sup>

The signal attenuation in a two compartment system described by the Kärger model can be understood by considering the total signal,  $\mathbf{S}$ , which can be described by a vector containing the contributions from the two compartments

## 6 Diffusion NMR for exchange

**Figure 6.2:** Signal attenuation for a two compartment system in exchange. Water in the two compartments have different apparent coefficients:  $D_1 = 2 \cdot 10^{-9} \text{ m}^2\text{s}^{-1}$  and  $D_2 = 8 \cdot 10^{-11} \text{ m}^2\text{s}^{-1}$ , as well as different average residence times,  $\tau_1 = 240 \text{ ms}$  and  $\tau_2 = 160 \text{ ms}$ . Signal attenuation curves are calculated from Eq. 6.2. Diffusion time,  $t_D$  is increased from 1 ms to 1 s.



$$\mathbf{S} = \begin{pmatrix} S_1 \\ S_2 \end{pmatrix}. \quad (6.6)$$

The signal evolution caused by diffusion effects is given by

$$\mathbf{S} = e^{-q^2 \mathbf{D} t_D} \mathbf{S}_0, \quad (6.7)$$

where

$$\mathbf{S}_0 = \begin{pmatrix} S_{0,1} \\ S_{0,2} \end{pmatrix} \quad (6.8)$$

is the total signal not affected by any attenuation and

$$\mathbf{D} = \begin{bmatrix} D_1 & 0 \\ 0 & D_2 \end{bmatrix}. \quad (6.9)$$

The signal evolution caused by exchange is given by

$$\mathbf{S} = e^{-\mathbf{K}t} \mathbf{S}_0, \quad (6.10)$$

where

$$\mathbf{K} = \begin{bmatrix} \frac{1}{\tau_1} & -\frac{1}{\tau_2} \\ -\frac{1}{\tau_1} & \frac{1}{\tau_2} \end{bmatrix}. \quad (6.11)$$

The Kärger model given in Eq. 6.2 can also be defined by a matrix exponential<sup>81</sup> in the following way

$$\mathbf{S} = e^{-(\mathbf{K}+q^2\mathbf{D})t_D}\mathbf{S}_0. \quad (6.12)$$

### 6.2.2 Filter exchange spectroscopy

Information on the exchange can also be obtained by extending the diffusion experiment into more dimensions.

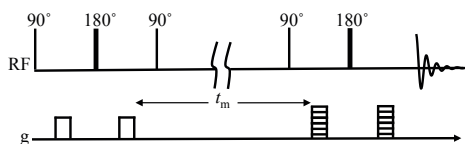


**Figure 6.3:** The FEXSY pulse sequence based on a double PGSE. A double diffusion encoding sequence, where the first block filters away the fast diffusing signal component. Exchange between the compartments occur in the mixing time  $t_m$  between the two diffusion encoding blocks. In the second encoding block diffusion weighting is increased by increasing the gradient strength.

Filter exchange spectroscopy (FEXSY) was first introduced by Åslund *et al.*<sup>11</sup> and is a modification of the diffusion exchange spectroscopy (DEXSY) experiment<sup>19</sup>. The FEXSY pulse sequence can be seen in Fig. 6.3. FEXSY is a double diffusion encoding sequence.<sup>82</sup> In the first diffusion encoding block, a pair of filter gradients, is applied. These attenuate signal mainly from the fast diffusing compartment, while most of the signal in the slow diffusing compartment is preserved. The second block is a normal diffusion encoding block with increasing gradient strengths. In between the two block there is the mixing time,  $t_m$ . In a case where all signal in the fast diffusing compartment is attenuated by the first block, the signal attenuation curve reflects the amount of slow diffusing molecules that exchanged sites with the fast diffusing molecules. The fraction of fast diffusing molecules,  $f_f$ , will increase with increasing  $t_m$  in the following way:

## 6 Diffusion NMR for exchange

$$f_f(t_m) = f_f^{eq} - [f_f^{eq} - f_f(0)]e^{-kt_m} \quad (6.13)$$

where  $f_f^{eq}$  is the extracellular fraction at equilibrium and  $f_f(0)$  is the extracellular fraction at  $t_m = 0$ .

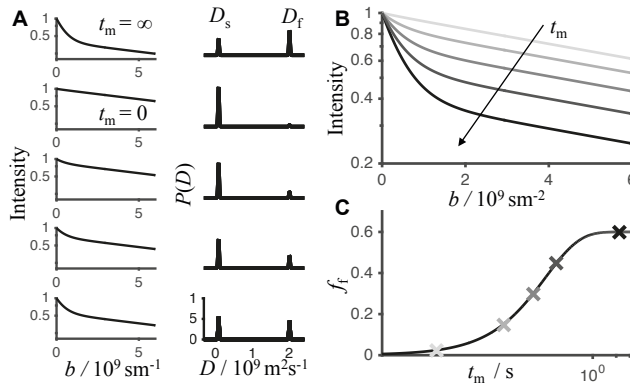


**Figure 6.4:** Calculated signal for FEXSY. (A) Signal attenuation at different mixing times,  $t_m$ , with corresponding probability distributions of the diffusion coefficients,  $P(D)$ . (B) Change of signal attenuation with increasing  $t_m$ . Curves have been normalized to all start at one. In reality the equilibrium attenuation (black curve) has the highest signal since no filter gradients are used. (C) Signal fraction of the fast component,  $f_f$  as a function  $t_m$ , following Eq. 6.13. The same diffusion coefficients and residence times was used as in Fig. 6.2.

In Fig. 6.4 signal attenuation curves from the FEXSY experiment is shown. The top row in the left panel shows the signal attenuation at equilibrium, acquired with the gradient strength in the first block equal to zero. After filtering the fast diffusing signal fraction  $f_f$  is removed but it will grow back with increasing  $t_m$ . It is assumed that exchange during the diffusion encoding block is small and can be neglected and hence signal attenuation will follow Eq. 6.1.

### 6.3 Accounting for differences in relaxation rates in FEXSY

In Paper IV we study a yeast cell suspension with a lower apparent diffusion coefficient of the intracellular water  $D_i$  and higher diffusion coefficient in the extracellular water  $D_e$ . The intracellular transverse relaxation  $T_{2i}$  is shorter than the extracellular  $T_{2e}$ . We



### 6.3 Accounting for differences in relaxation rates in FEXSY

use a modulated FEXSY sequence, based on a double stimulated echo to adjust for short  $T_2$  relaxation times. A schematic of the sequence is shown in 6.5A.

To adjust for different  $T_2$  values in the two compartments, a second experiment was combined with the FEXSY experiment. The second experiment was a normal PGSE pulse sequence with varying echo time and constant diffusion time. The varying echo time makes it possible to correlate  $T_2$  and  $D$ .<sup>83–85</sup>

#### 6.3.1 Operator analysis for signal evolution

The Kärger model shown in Eq. 6.2 can be modified to include effect of relaxation differences between the compartments.<sup>86</sup> Eq. 6.12 can also be modified to include relaxation by adding the relaxation matrix

$$\mathbf{R} = \begin{pmatrix} R_{2i} & 0 \\ 0 & R_{2e} \end{pmatrix} \quad (6.14)$$

to the exponential, where  $R_{2i} = 1/T_{2i}$  and  $R_{2e} = 1/T_{2e}$ . During the diffusion encoding, the operator acting on  $\mathbf{S}_0$  is given by

$$O_{\mathbf{P2}} = e^{-(\mathbf{R}+\mathbf{K}+q^2\mathbf{D})t_D}. \quad (6.15)$$

For PGSE, when there is relaxation time differences between the two compartments, the time before and after  $t_D$  will also contribute to the signal evolution and the operator acting on the signal is given by

$$O_{\mathbf{P1}} = e^{-\frac{1}{2}(\mathbf{R}+\mathbf{K})(t_E-t_D)}. \quad (6.16)$$

For PGSE the signal evolution is given by

$$\mathbf{S}_{\text{PGSE}} = O_{\mathbf{P1}}O_{\mathbf{P2}}O_{\mathbf{P1}}\mathbf{S}_0. \quad (6.17)$$

This type of signal evolution representation is common also in spectroscopic solid state

## 6 Diffusion NMR for exchange

experiments.<sup>87</sup> The signal evolution for the FEXSY experiment can be represented in a similar way (see Paper IV).

In Fig. 6.5B the different operators acting on the signal during the FEXSY sequence are represented by different coloured blocks and the different patterned blocks show when exchange, relaxation and diffusion is affecting the signal evolution.

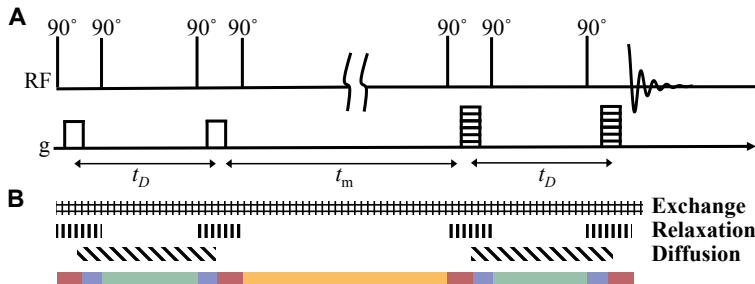


**Figure 6.5:** (A) FEXSY based on a double stimulated echo. (B) The different patterned blocks mark the time intervals when the signal is subjected to the evolution operators for exchange,  $T_2$ -relaxation, and diffusion, respectively. The coloured blocks show the time intervals during which the different operators apply: during the red block there is exchange and relaxation affecting the signal evolution; during the blue block there is exchange, relaxation and diffusion; during green there is diffusion and exchange; and during yellow there is only exchange.

The effects of exchange in the presence of different relaxation times between two compartments can cause rather complex signal behaviours. Fig. 6.6 displays the signal evolution for the FEXSY sequence shown in Fig. 6.5. For the calculation of the signal evolutions,  $T_1$  relaxation was ignored and there was no diffusion weighting in the second diffusion encoding block.

By comparing the signal at short and long mixing times, a small increase in the total signal intensity can be observed at long  $t_m$ . This can first seem counter-intuitive, since longer experimental times should not cause an increase in the signal, rather the opposite, and in this case where  $T_1$  relaxation is ignored during  $t_m$ , the two experimental times should give the same signal intensity. However, the reason for increasing total signal intensity is that long  $t_m$  allows the water to diffuse to the extracellular compartment. This leads to a higher extracellular signal fraction, resulting in less signal loss due to  $T_2$  relaxation during the second diffusion encoding block. For our yeast cell systems the increased signal intensity at longer  $t_m$  can not be shown experimentally. This is

### 6.3 Accounting for differences in relaxation rates in FEXSY

because large differences in  $t_m$  is needed to see the effect and in reality  $T_1$  relaxation will decrease the signal during this time. However, there will be an effect on the measured signals fractions, which is discussed more in Paper IV.

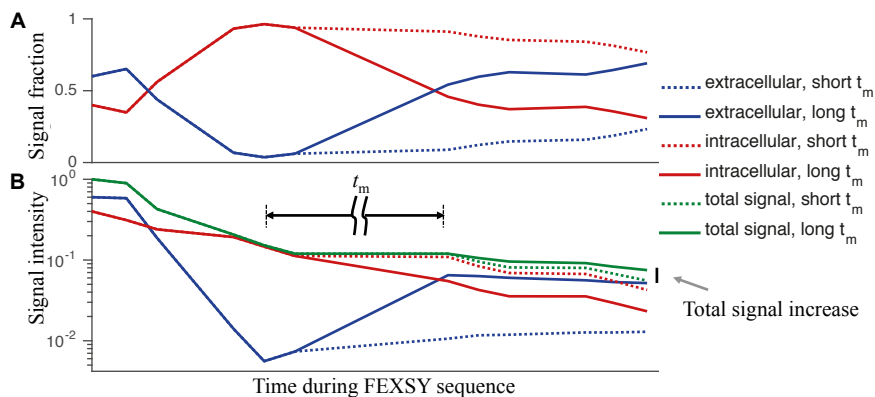


**Figure 6.6:** Signal evolution during the FEXSY sequence shown in Fig. 6.5. (A) Signal fractions of extracellular (blue) and intracellular (red) water. At short  $t_m$  the intracellular fraction (red dotted line) is much higher than the extracellular fraction (blue dotted line) at the end of the sequence. For long  $t_m$ , extracellular fraction (blue solid line) is higher than the intracellular fraction (red solid lines). (B) The signal intensities during the FEXSY sequence. Here it can clearly be seen that during the long  $t_m$  (solid lines), there is more mixing between the two compartments than for the short  $t_m$ . This causes a increase in the total signal in the end of the sequence (green lines).



# 7

## Concluding remarks

NMR diffusion is a powerful technique for probing the translational motion of water molecules. The diffusion NMR signal can reveal information about the microscopic structure of porous materials. The technique is used as a diagnostic tool and can image connecting structures in the brain.

The novel diffusion NMR methods presented in Paper I-III in this thesis, reveal information on microscopic structures, which is not attainable with conventional diffusion methods used in the clinic today. With these new methods, otherwise confounding influence of different orientations of the microscopic structures, is removed. We show in well characterised systems that these novel methods can reveal underlying microscopic structures, and that the microscopic diffusion tensor can be quantified.

Biological tissue is far more complicated than liquid crystals, though. Also, as was shown in Paper IV, relaxation and exchange can make the interpretation of the diffusion NMR signal quite complicated. However, the use of simple model systems such as liquid crystals and yeast cell suspensions is, in my opinion, great for validation of diffusion NMR methods.

The hope is of course that the methods can become useful in a clinical setting, as a tool for improved diagnostics. With this in mind, the method presented in Paper II was optimized for a clinical system. Since that publication, the same method has been applied *in vivo* to study cell structure in brain tumours.<sup>88</sup>



# References

- [1] Paul T. Callaghan. *Translational Dynamics and Magnetic Resonance: Principles of Pulsed Gradient Spin Echo NMR*. Oxford University Press, 2011.
- [2] P. T. Callaghan and O. Soderman. Examination of the lamellar phase of aerosol OT/water using pulsed field gradient nuclear magnetic resonance. *The Journal of Physical Chemistry*, 87(10):1737–1744, 1983.
- [3] M. D. Hürlimann, K. G. Helmer, L. L. Latour, and C. H. Sotak. Restricted Diffusion in Sedimentary Rocks. Determination of Surface-Area-to-Volume Ratio and Surface Relaxivity. *Journal of Magnetic Resonance, Series A*, 111(2):169–178, 1994.
- [4] Daniel Topgaard and Olle Söderman. Self-Diffusion in Two- and Three-Dimensional Powders of Anisotropic Domains: An NMR Study of the Diffusion of Water in Cellulose and Starch. *The Journal of Physical Chemistry B*, 106(46):11887–11892, 2002.
- [5] Denis Le Bihan. Looking into the functional architecture of the brain with diffusion MRI. *Nature Reviews Neuroscience*, 4(6):469–480, 2003.
- [6] Derek K. Jones. *Diffusion MRI*. Oxford University Press, 2011.
- [7] Christian Beaulieu. The basis of anisotropic water diffusion in the nervous system – a technical review. *NMR in Biomedicine*, 15(7-8): 435–455, 2002.
- [8] Marek Kubicki, Robert McCarley, Carl-Fredrik Westin, Hae-Jeong Park, Stephan Maier, Ron Kikinis, Ferenc A. Jolesz, and Martha E. Shenton. A review of diffusion tensor imaging studies in schizophrenia. *Journal of Psychiatric Research*, 41(1):15–30, 2007.
- [9] G. M. Preston and P. Agre. Isolation of the cDNA for erythrocyte integral membrane protein of 28 kilodaltons: member of an ancient channel family. *Proc. Natl. Acad. Sci. U.S.A.*, 88(24):11110–11114, 1991.
- [10] Gregory M. Preston, Tiziana Piazza Carroll, William B. Guggino, and Peter Agre. Appearance of Water Channels in *Xenopus* Oocytes Expressing Red Cell CHIP28 Protein. *Science*, 256(5055):385–387, 1992.
- [11] Ingrid Åslund, Agnieszka Nowacka, Markus Nilsson, and Daniel Topgaard. Filter-exchange PGSE NMR determination of cell membrane permeability. *J. Magn. Reson.*, 200(2):291–295, 2009.
- [12] Peter Atkins. *Physical Chemistry*. Oxford University Press, 8th edition, 2006.
- [13] D. Fennell Evans and Håkan Wennerström. *The Colloidal Domain: Where Physics, Chemistry, Biology and Technology Meet*. Wiley-VCH, New York, 2nd ed. edition, 1999.
- [14] William S. Price. Pulsed-field gradient nuclear magnetic resonance as a tool for studying translational diffusion: Part 1. Basic theory. *Concepts in Magnetic Resonance*, 9(5):299–336, 1997.
- [15] J. E. Tanner and E. O. Stejskal. Restricted Self-Diffusion of Protons in Colloidal Systems by the Pulsed-Gradient, Spin-Echo Method. *J. Chem. Phys.*, 49(4):1768–1777, 1968.
- [16] D. E. Woessner. N.M.R. SPIN-ECHO SELF-DIFFUSION MEASUREMENTS ON FLUIDS UNDERGOING RESTRICTED DIFFUSION. *The Journal of Physical Chemistry*, 67(6):1365–1367, 1963.
- [17] E. O. Stejskal. Use of Spin Echoes in a Pulsed Magnetic-Field Gradient to Study Anisotropic, Restricted Diffusion and Flow. *J. Chem. Phys.*, 43(10):3597–3603, 1965.
- [18] P J Basser, J Mattiello, and D LeBihan. MR diffusion tensor spectroscopy and imaging. *Biophysical Journal*, 66(1):259–267, 1994.
- [19] P T Callaghan and I Furó. Diffusion-diffusion correlation and exchange as a signature for local order and dynamics. *J. chem. phys.*, 120(8):4032–8, 2004.
- [20] P. T. Callaghan and M. E. Komlos. Locally anisotropic motion in a macroscopically isotropic system: displacement correlations measured using double pulsed gradient spin-echo NMR. *Magnetic Resonance in Chemistry*, 40(13):S15–S19, 2002.
- [21] Monika Schönhoff and Olle Söderman. PFG-NMR Diffusion as a Method To Investigate the Equilibrium Adsorption Dynamics of Surfactants at the Solid/Liquid Interface. *J. Phys. Chem. B*, 101(41): 8237–8242, 1997.
- [22] I. I. Rabi, J. R. Zacharias, S. Millman, and P. Kusch. A New Method of Measuring Nuclear Magnetic Moment. *Physical Review*, 53(4): 318–318, 1938.
- [23] F. Bloch. Nuclear Induction. *Physical Review*, 70(7-8):460–474, 1946.
- [24] E. M. Purcell, H. C. Torrey, and R. V. Pound. Resonance Absorption by Nuclear Magnetic Moments in a Solid. *Physical Review*, 69(1-2): 37–38, 1946.
- [25] James Keeler. *Understanding NMR spectroscopy*. Wiley, 2010.
- [26] Donald W. McRobbie, Elizabeth A. Moore, Martin J. Graves, and Martin R. Prince. *MRI from Picture to Proton*. Cambridge University Press, 2006.
- [27] Malcolm H. Levitt. *Spin Dynamics: Basics of Nuclear Magnetic Resonance*. John Wiley & Sons, 2008.
- [28] E. L. Hahn. Spin Echoes. *Physical Review*, 80(4):580–594, 1950.
- [29] William S. Price. *NMR Studies of Translational Motion: Principles and Applications*. Cambridge University Press, 2009.

## REFERENCES

---

- [30] Olle Söderman, William S. Price, Monika Schönhoff, and Daniel Topgaard. NMR diffusometry applied to liquids. *Journal of Molecular Liquids*, 156(1):38–44, 2010.
- [31] P. J. Basser and C. Pierpaoli. Microstructural and physiological features of tissues elucidated by quantitative-diffusion-tensor MRI. *Journal of Magnetic Resonance. Series B*, 111(3):209–219, 1996.
- [32] E. O. Stejskal and J. E. Tanner. Spin Diffusion Measurements: Spin Echoes in the Presence of a Time-Dependent Field Gradient. *J. Chem. Phys.*, 42(1):288–292, 1965.
- [33] J. E. Tanner. Use of the Stimulated Echo in NMR Diffusion Studies. *J. Chem. Phys.*, 52(5):2523–2526, 1970.
- [34] Jörg Kärgel and Wilfried Heink. The propagator representation of molecular transport in microporous crystallites. *Journal of Magnetic Resonance (1969)*, 51(1):1–7, 1983.
- [35] P. P. Mitra and B. I. Halperin. Effects of Finite Gradient-Pulse Widths in Pulsed-Field-Gradient Diffusion Measurements. *Journal of Magnetic Resonance, Series A*, 113(1):94–101, 1995.
- [36] Ingrid Åslund and Daniel Topgaard. Determination of the self-diffusion coefficient of intracellular water using PGSE NMR with variable gradient pulse length. *J. Magn. Reson.*, 201(2):250–254, 2009.
- [37] Frederik B. Laun and Tristan A. Kuder. Diffusion pore imaging with generalized temporal gradient profiles. *Magnetic Resonance Imaging*, 31(7):1236–1244, 2013.
- [38] Stefan Hertel, Mark Hunter, and Petrik Galvosas. Magnetic resonance pore imaging, a tool for porous media research. *Physical Review E*, 87(3):030802, 2013.
- [39] Paul Callaghan. *Principles of Nuclear Magnetic Resonance Microscopy*. Oxford University Press, Oxford, 1st ed. edition, 1991.
- [40] Maria Nyblom, Fredrik Öberg, Karin Lindkvist-Petersson, Karin Hallgren, Heather Findlay, Jennie Wikström, Anders Karlsson, Orjan Hansson, Paula J. Booth, Roslyn M. Bill, Richard Neutze, and Kristina Hedfalk. Exceptional overproduction of a functional human membrane protein. *Protein Expr. Purif.*, 56(1):110–120, 2007.
- [41] Krister Holmberg, Bo Jönsson, Bengt Kronberg, and Björn Lindman. *Surfactants and Polymers in Aqueous Solution, 2nd ed.* Wiley, 2003.
- [42] Jacob N. Israelachvili, D. John Mitchell, and Barry W. Ninham. Theory of self-assembly of hydrocarbon amphiphiles into micelles and bilayers. *Journal of the Chemical Society, Faraday Transactions 2: Molecular and Chemical Physics*, 72(0):1525–1568, 1976.
- [43] G. J. T Tiddy. Surfactant-water liquid crystal phases. *Physics Reports*, 57(1):1–46, 1980.
- [44] J. Rogers and P. A. Winsor. Change in the optic sign of the lamellar phase (G) in the aerosol OT/water system with composition or temperature. *Journal of Colloid and Interface Science*, 30(2):247–257, 1969.
- [45] Nissim Garti, Dima Libster, and Abraham Aserin. Lipid polymorphism in lyotropic liquid crystals for triggered release of bioactives. *Food & Function*, 3(7):700–713, 2012.
- [46] Tiago Mendes Ferreira, Diana Bernin, and Daniel Topgaard. Chapter Three - NMR Studies of Nonionic Surfactants. In Graham A. Webb, editor, *Annual Reports on NMR Spectroscopy*, volume 79, pages 73–127. Academic Press, 2013.
- [47] G. E. Pake. Nuclear Resonance Absorption in Hydrated Crystals: Fine Structure of the Proton Line. *The Journal of Chemical Physics*, 16(4):327–336, 1948.
- [48] J. E. Tanner. Intracellular diffusion of water. *Archives of Biochemistry and Biophysics*, 224(2):416–428, 1983.
- [49] Matthew D. Silva, Karl G. Helmer, Jing-Huei Lee, Sam S. Han, Charles S. Springer Jr., and Christopher H. Sotak. Deconvolution of Compartmental Water Diffusion Coefficients in Yeast-Cell Suspensions Using Combined T1 and Diffusion Measurements. *Journal of Magnetic Resonance*, 156(1):52–63, 2002.
- [50] Jing-Huei Lee and Charles S. Springer. Effects of equilibrium exchange on diffusion-weighted NMR signals: The diffusigraphic “shutter-speed”. *Magnetic Resonance in Medicine*, 49(3):450–458, 2003.
- [51] Carin Malmberg, Martin Sjöbeck, Sara Brockstedt, Elisabeth Englund, Olle Söderman, and Daniel Topgaard. Mapping the intracellular fraction of water by varying the gradient pulse length in q-space diffusion MRI. *Journal of Magnetic Resonance*, 180(2):280–285, 2006.
- [52] Juan I. Castrillo, Leo A. Zeef, David C. Hoyle, Nianshu Zhang, Andrew Hayes, David CJ Gardner, Michael J. Cornell, June Petty, Luke Hakes, Leanne Wardleworth, Bharat Rash, Marie Brown, Warwick B. Dunn, David Broadhurst, Kerry O’Donoghue, Svenja S. Hester, Tom PJ Dunkley, Sarah R. Hart, Neil Swainston, Peter Li, Simon J. Gaskell, Norman W. Paton, Kathryn S. Lilley, Douglas B. Kell, and Stephen G. Oliver. Growth control of the eukaryote cell: a systems biology study in yeast. *Journal of Biology*, 6:4, 2007.
- [53] A. Goffeau, B. G. Barrell, H. Bussey, R. W. Davis, B. Dujon, H. Feldmann, F. Galibert, J. D. Hoheisel, C. Jacq, M. Johnston, E. J. Louis, H. W. Mewes, Y. Murakami, P. Philippsen, H. Tettelin, and S. G. Oliver. Life with 6000 Genes. *Science*, 274(5287):546–567, 1996.
- [54] Thomas H. Haines. Water transport across biological membranes. *FEBS Lett.*, 346(1):115–122, 1994.
- [55] Landon S King, Masato Yasui, and Peter Agre. Aquaporins in health and disease. *Molecular Medicine Today*, 6(2):60–65, 2000.
- [56] Rebecca E. Day, Philip Kitchen, David S. Owen, Charlotte Bland, Lindsay Marshall, Alex C. Conner, Roslyn M. Bill, and Matthew T. Conner. Human aquaporins: Regulators of transcellular water flow. *Biochimica et Biophysica Acta (BBA) - General Subjects*, 1840(5):1492–1506, 2014.



- [57] Jian Wang, Li Feng, Zhitu Zhu, Minghuan Zheng, Diane Wang, Zhihong Chen, and Hongzhi Sun. Aquaporins as diagnostic and therapeutic targets in cancer: How far we are? *Journal of Translational Medicine*, 13:96, 2015.
- [58] M.e. Komlosh, M.j. Lizak, F. Horkay, R.z. Freidlin, and P.j. Bassar. Observation of microscopic diffusion anisotropy in the spinal cord using double-pulsed gradient spin echo MRI. *Magnetic Resonance in Medicine*, 59(4):803–809, 2008.
- [59] Partha P. Mitra. Multiple wave-vector extensions of the NMR pulsed-field-gradient spin-echo diffusion measurement. *Physical Review B*, 51(21):15074–15078, 1995.
- [60] Marco Lawrenz, Martin A. Koch, and Jürgen Finsterbusch. A tensor model and measures of microscopic anisotropy for double-wave-vector diffusion-weighting experiments with long mixing times. *Journal of Magnetic Resonance*, 202(1):43–56, 2010.
- [61] Noam Shemesh and Yoram Cohen. Microscopic and compartment shape anisotropies in gray and white matter revealed by angular bipolar double-PFG MR. *Magnetic Resonance in Medicine*, 65(5):1216–1227, 2011.
- [62] Susumu Mori and Peter C. M. Van Zijl. Diffusion Weighting by the Trace of the Diffusion Tensor within a Single Scan. *Magnetic Resonance in Medicine*, 33(1):41–52, 1995.
- [63] Robin A. de Graaf, Kees P.J. Braun, and Klaas Nicolay. Single-shot diffusion trace 1h NMR spectroscopy. *Magnetic Resonance in Medicine*, 45(5):741–748, 2001.
- [64] Julien Valette, Céline Giraudeau, Charlotte Marchadour, Boucif Djemai, Françoise Geffroy, Mohamed Ahmed Ghaly, Denis Le Bihan, Philippe Hantraye, Vincent Lebon, and Franck Lethimonnier. A new sequence for single-shot diffusion-weighted NMR spectroscopy by the trace of the diffusion tensor. *Magnetic Resonance in Medicine*, 68(6):1705–1712, 2012.
- [65] David D. Laws, Hans-Marcus L. Bitter, and Alexej Jerschow. Solid-State NMR Spectroscopic Methods in Chemistry. *Angewandte Chemie International Edition*, 41(17):3096–3129, 2002.
- [66] Daniel Topgaard. Isotropic diffusion weighting in PGSE NMR: Numerical optimization of the q-MAS PGSE sequence. *Microporous and Mesoporous Materials*, 178:60–63, 2013.
- [67] Mads Bak and Niels Chr Nielsen. REPULSION, A Novel Approach to Efficient Powder Averaging in Solid-State NMR. *Journal of Magnetic Resonance*, 125(1):132–139, 1997.
- [68] D.k. Jones, M.a. Horsfield, and A. Simmons. Optimal strategies for measuring diffusion in anisotropic systems by magnetic resonance imaging. *Magnetic Resonance in Medicine*, 42(3):515–525, 1999.
- [69] Daniel Topgaard. Isotropic diffusion weighting using a triple-stimulated echo pulse sequence with bipolar gradient pulse pairs. *Microporous and Mesoporous Materials*, 205:48–51, 2015.
- [70] Mark L. Zeidel, Suresh V. Ambudkar, Barbara L. Smith, and Peter Agre. Reconstitution of functional water channels in liposomes containing purified red cell CHIP28 protein. *Biochemistry*, 31(33):7436–7440, 1992.
- [71] T. Conlon and R. Outhred. Water diffusion permeability of erythrocytes using an NMR technique. *Biochim. Biophys. Acta*, 288(2):354–361, 1972.
- [72] C. Labadie, J. H. Lee, G. Vetek, and C. S. Springer. Relaxographic Imaging. *J. Magn. Reson. B*, 105(2):99–112, 1994.
- [73] Yajie Zhang, Marie Poirier-Quinot, Charles S. Springer, and James A. Balschi. Active Trans-Plasma Membrane Water Cycling in Yeast Is Revealed by NMR. *Biophys. J.*, 101(11):2833–2842, 2011.
- [74] B. Balinov, B. Jonsson, P. Linse, and O. Soderman. The NMR Self-Diffusion Method Applied to Restricted Diffusion. Simulation of Echo Attenuation from Molecules in Spheres and between Planes. *Journal of Magnetic Resonance, Series A*, 104(1):17–25, 1993.
- [75] Jörg Kärger. NMR self-diffusion studies in heterogeneous systems. *Adv. Colloid Interface Sci.*, 23:129–148, 1985.
- [76] Jan Andrasko. Water diffusion permeability of human erythrocytes studied by a pulsed gradient NMR technique. *Biochim. Biophys. Acta*, 428(2):304–311, 1976.
- [77] Josef Pfeuffer, Ulrich Flögel, Wolfgang Dreher, and Dieter Leibfritz. Restricted diffusion and exchange of intracellular water: theoretical modelling and diffusion time dependence of 1h NMR measurements on perfused glial cells. *NMR Biomed.*, 11(1):19–31, 1998.
- [78] Yiftach Roth, Aharon Ocherashvilli, Dianne Daniels, Jesus Ruiz-Cabello, Stephan E. Maier, Arie Orenstein, and Yael Mardor. Quantification of water compartmentation in cell suspensions by diffusion-weighted and T2-weighted MRI. *Magn. Reson. Imaging*, 26(1):88–102, 2008.
- [79] C. S. Johnson. Effects of Chemical Exchange in Diffusion-Ordered 2d NMR Spectra. *Journal of Magnetic Resonance, Series A*, 102(2):214–218, 1993.
- [80] W S Price, A V Barzykin, K Hayamizu, and M Tachiya. A model for diffusive transport through a spherical interface probed by pulsed-field gradient NMR. *Biophys. J.*, 74(5):2259–2271, 1998.
- [81] M. Nilsson, E. Alerstam, R. Wirestam, F. Ståhlberg, S. Brockstedt, and J. Lätt. Evaluating the accuracy and precision of a two-compartment Kärger model using Monte Carlo simulations. *Journal of Magnetic Resonance*, 206(1):59–67, 2010.
- [82] Noam Shemesh, Sune N. Jespersen, Daniel C. Alexander, Yoram Cohen, Ivana Drobňjak, Tim B. Dyrby, Jürgen Finsterbusch, Martin A. Koch, Tristan Kuder, Fredrik Laun, Marco Lawrenz, Henrik Lundell, Partha P. Mitra, Markus Nilsson, Evren Özarslan, Daniel Topgaard, and Carl-Fredrik Westin. Conventions and nomenclature for double diffusion encoding NMR and MRI. *Magnetic Resonance in Medicine*, 75(1):82–87, 2016.

## REFERENCES

---

- [83] Dagmar van Dusschoten, P. A. Dejager, and H. Vanas. Extracting Diffusion Constants from Echo-Time-Dependent PFG NMR Data Using Relaxation-Time Information. *Journal of Magnetic Resonance, Series A*, 116(1):22–28, 1995.
- [84] Sharon Peled, David G. Cory, Stephen A. Raymond, Daniel A. Kirschner, and Ferenc A. Jolesz. Water Diffusion, T2, and Compartmentation in Frog Sciatic Nerve. *Magnetic resonance in medicine : official journal of the Society of Magnetic Resonance in Medicine / Society of Magnetic Resonance in Medicine*, 42(5):911–918, 1999.
- [85] M. D Hürlimann and L Venkataramanan. Quantitative Measurement of Two-Dimensional Distribution Functions of Diffusion and Relaxation in Grossly Inhomogeneous Fields. *Journal of Magnetic Resonance*, 157(1):31–42, 2002.
- [86] J. Kärger. Der Einfluß der Zweibereichdiffusion auf die Spinechodämpfung unter Berücksichtigung der Relaxation bei Messungen mit der Methode der gepulsten Feldgradienten. *Annalen der Physik*, 482(1):107–109, 1971.
- [87] K. Schmidt-Rohr and H. W. Spiess. *Multidimensional Solid-State NMR and Polymers*. Academic Press, 1994.
- [88] Filip Szczepankiewicz, Samo Lasic, Danielle van Westen, Pia C. Sundgren, Elisabet Englund, Carl-Fredrik Westin, Freddy Ståhlberg, Jimmy Lätt, Daniel Topgaard, and Markus Nilsson. Quantification of microscopic diffusion anisotropy disentangles effects of orientation dispersion from microstructure: Applications in healthy volunteers and in brain tumors. *NeuroImage*, 104:241–252, 2015.



**LUND**  
UNIVERSITY

Faculty of Science  
Center for Chemistry and Chemical Engineering  
ISBN 978-91-7623-824-0 (print)  
ISBN 978-91-7623-825-7 (pdf)

